UNIVERSIDADE FEDERAL DO PARANÁ

LORENA MARCELINO DOS SANTOS

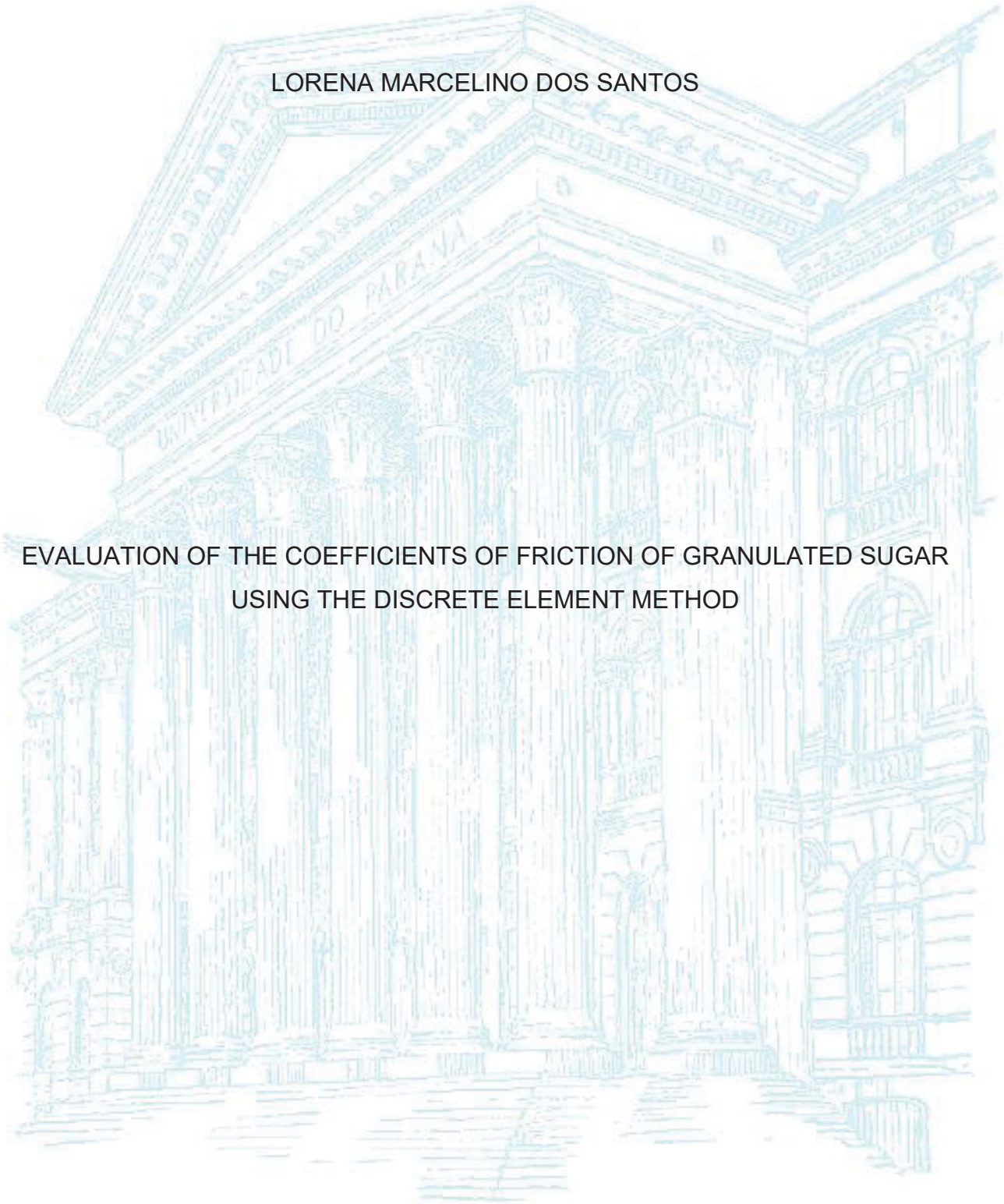

EVALUATION OF THE COEFFICIENTS OF FRICTION OF GRANULATED SUGAR USING THE DISCRETE ELEMENT METHOD

CURITIBA

2022

LORENA MARCELINO DOS SANTOS

EVALUATION OF THE COEFFICIENTS OF FRICTION OF GRANULATED SUGAR USING THE DISCRETE ELEMENT METHOD

Dissertação submetida ao Programa de Pós-Graduação em Engenharia Química, do Setor de Tecnologia da Universidade Federal do Paraná, como requisito à obtenção de grau de Mestre em Engenharia Química.

Orientador: Prof. Luiz Fernando de Lima Luz Jr.
Coorientador: Prof. Dr. Fernando Augusto Pedersen Voll

CURITIBA

2022

DADOS INTERNACIONAIS DE CATALOGAÇÃO NA PUBLICAÇÃO (CIP)
UNIVERSIDADE FEDERAL DO PARANÁ
SISTEMA DE BIBLIOTECAS – BIBLIOTECA CIÊNCIA E TECNOLOGIA

Santos, Lorena Marcelino dos
Evaluation of the coefficients of friction of granulated sugar using the discrete element method. / Lorena Marcelino dos Santos. – Curitiba, 2022.
1 recurso on-line : PDF.

Dissertação (Mestrado) – Universidade Federal do Paraná, Setor de Tecnologia, Programa de Pós-Graduação em Engenharia Química.

Orientador: Prof. Dr. Luiz Fernando de Lima Luz Jr.
Coorientador: Prof. Dr. Fernando Augusto Pedersen Voll

1. Açúcar. 2. Materiais granulares. 3.Método dos elementos discretos. I. Luz Jr., Luiz Fernando de Lima. II. Voll, Fernando Augusto Pedersen. III. Universidade Federal do Paraná. Programa de Pós-Graduação em Engenharia Química. IV. Título.

Bibliotecária: Roseny Rivelini Morciani CRB-9/1585

ATA Nº166

ATA DE SESSÃO PÚBLICA DE DEFESA DE MESTRADO PARA A OBTENÇÃO DO GRAU DE MESTRA EM ENGENHARIA QUÍMICA

No dia vinte e nove de setembro de dois mil e vinte e dois às 14:00 horas, na sala Auditório I, Prédio da Engenharia Química no Centro Politécnico da UFPR, foram instaladas as atividades pertinentes ao rito de defesa de dissertação da mestranda **LORENA MARCELINO DOS SANTOS**, intitulada**: EVALUATION OF THE COEFFICIENTS OF FRICTION OF GRANULATED SUGAR USING THE DISCRETE ELEMENTS METHOD**, sob orientação do Prof. Dr. LUIZ FERNANDO DE LIMA LUZ JUNIOR. A Banca Examinadora, designada pelo Colegiado do Programa de Pós-Graduação ENGENHARIA QUÍMICA da Universidade Federal do Paraná, foi constituída pelos seguintes Membros: LUIZ FERNANDO DE LIMA LUZ JUNIOR (UNIVERSIDADE FEDERAL DO PARANÁ), ELITON FONTANA (UNIVERSIDADE FEDERAL DO PARANÁ), EMERSON MARTIM (PONTIFÍCIA UNIVERSIDADE CATÓLICA DO PARANÁ). A presidência iniciou os ritos definidos pelo Colegiado do Programa e, após exarados os pareceres dos membros do comitê examinador e da respectiva contra argumentação, ocorreu a leitura do parecer final da banca examinadora, que decidiu pela APROVAÇÃO. Este resultado deverá ser homologado pelo Colegiado do programa, mediante o atendimento de todas as indicações e correções solicitadas pela banca dentro dos prazos regimentais definidos pelo programa. A outorga de título de mestra está condicionada ao atendimento de todos os requisitos e prazos determinados no regimento do Programa de Pós-Graduação. Nada mais havendo a tratar a presidência deu por encerrada a sessão, da qual eu, LUIZ FERNANDO DE LIMA LUZ JUNIOR, lavrei a presente ata, que vai assinada por mim e pelos demais membros da Comissão Examinadora.

CURITIBA, 29 de Setembro de 2022.

Assinatura Eletrônica
29/09/2022 15:53:23.0
LUIZ FERNANDO DE LIMA LUZ JUNIOR
Presidente da Banca Examinadora

Assinatura Eletrônica
29/09/2022 15:49:42.0
ELITON FONTANA
Avaliador Interno (UNIVERSIDADE FEDERAL DO PARANÁ)

Assinatura Eletrônica
29/09/2022 15:48:26.0
EMERSON MARTIM
Avaliador Externo (PONTIFÍCIA UNIVERSIDADE CATÓLICA DO PARANÁ)

TERMO DE APROVAÇÃO

Os membros da Banca Examinadora designada pelo Colegiado do Programa de Pós-Graduação ENGENHARIA QUÍMICA da Universidade Federal do Paraná foram convocados para realizar a arguição da dissertação de Mestrado de **LORENA MARCELINO DOS SANTOS** intitulada: **EVALUATION OF THE COEFFICIENTS OF FRICTION OF GRANULATED SUGAR USING THE DISCRETE ELEMENTS METHOD**, sob orientação do Prof. Dr. LUIZ FERNANDO DE LIMA LUZ JUNIOR, que após terem inquirido a aluna e realizada a avaliação do trabalho, são de parecer pela sua APROVAÇÃO no rito de defesa.

A outorga do título de mestra está sujeita à homologação pelo colegiado, ao atendimento de todas as indicações e correções solicitadas pela banca e ao pleno atendimento das demandas regimentais do Programa de Pós-Graduação.

CURITIBA, 29 de Setembro de 2022.

Assinatura Eletrônica
29/09/2022 15:53:23.0
LUIZ FERNANDO DE LIMA LUZ JUNIOR
Presidente da Banca Examinadora

Assinatura Eletrônica
29/09/2022 15:49:42.0
ELITON FONTANA
Avaliador Interno (UNIVERSIDADE FEDERAL DO PARANÁ)

Assinatura Eletrônica
29/09/2022 15:48:26.0
EMERSON MARTIM
Avaliador Externo (PONTIFÍCIA UNIVERSIDADE CATÓLICA DO PARANÁ)

ACKNOWLEDGMENTS

Several difficulties confronted me on my journey to completing my master's degree. It was a period highlighted by tremendous commitment and effort, as I shared my time between education and work. This work could not have been finished without the assistance of various personalities who have gone through my life and for whom I am eternally grateful.

First and foremost, I thank God for giving me the courage to face each daily difficulty during this study assignment while remaining healthy and strong enough to complete it.

I would like to express my gratitude to my advisor Professor Doctor Luiz Fernando de Lima Luz Jr. and co-advisor Professor Doctor Fernando Augusto Pedersen Voll for their extraordinary presence and support during the work's progress, including for their encouragement and time commitment to my research project. Also, thanks to Lucas Fedalto Sartori, a research colleague who was always proactive in the extra activities supporting me with the study's development.

I also want to express my gratitude to the Federal University of Paraná and all the professors in my course for their excellent instruction.

I am grateful to my family for their unquestioning support throughout my life.

Finally, I would like to express my heartfelt thanks to my friends who supported and believed in me during this journey.

RESUMO

O método dos elementos discretos (DEM) trata-se de uma técnica matemática descritiva do comportamento de partículas. A utilização dele está associada à sua capacidade descritiva de sistemas granulares similarmente a testes reais. Elaborar modelos capazes de descrever e prever as principais influências em sistemas particulados que diminuem o tempo e o custo de novos projetos. Os materiais particulares estão presentes em inúmeros segmentos na indústria como a química, farmacêutica, alimentos, bebidas e entre outras. O entendimento das propriedades e comportamento de misturas granulares são de extrema importância para o desenvolvimento de novos produtos, dessa maneira, podem resultar as melhores condições experimentais para a elaboração do estudo. Neste presente trabalho, será estudado um dos principais commodities da indústria alimentícia, o açúcar, neste caso o granulado (GUARANI®), visando buscar os coeficientes de atrito estático e de rolamento dele. Para a obtenção dos dados experimentais realizou-se um teste experimental em um tambor rotativo, realizando a sua reprodução via simulação (LIGGGHTS®), com base nos modelos propostos pelos estudos de Benchmark, com o modelo de contato de Hertz-Mindlin com histórico de rolamento. Com os estudos realizados, concluiu-se que o software apresenta capacidade de reprodução dos dados de maneira eficaz, desde que as condições de contorno sejam aplicadas corretamente, os coeficientes de fricção do açúcar cristal são caracterizados por uma faixa de valores, sendo 0,75 a 1 para o estático e 1 para o de rolamento.

Palavras-chave: DEM. LIGGGHTS®. Materiais granulares. Açúcar. Hertz-Mindlin.

ABSTRACT

The discrete element method (DEM) is a mathematical technique describing particles' behavior. Its use is related to its capacity to define granular systems that are similar to real-world testing. Can create models capable of characterizing and forecasting the major impacts on particle systems to reduce project time and cost. Chemicals, pharmaceuticals, food, beverages, and other materials are examples of materials used in the industry. Understanding the physics and behavior of granular mixes is critical in the creation of innovative products. This allows the ideal experimental conditions for the research to be established. This project will look at one of the most important commodities in the food industry: sugar, specifically granulated sugar (GUARANI®), which will be investigated to determine its static and rolling friction coefficients. To obtain the experimental data, an experimental test was performed on a rotating drum, with its reproduction accomplished by simulation (LIGGGHTS®), using the Hertz-Mindlin contact model with rolling history, based on the models presented by the Benchmark studies. The research found that the program can efficiently recreate data if the boundary conditions are implemented appropriately. For crystal sugar, the friction coefficients were characterized between 0.75 and 1 for static and 1 for rolling.

Keywords: DEM. LIGGGHTS® Granular materials. Sugar. Hertz-Mindlin.

ILLUSTRATIONS LIST

TABLES LIST

LIST OF ABBREVIATIONS AND ACRONYMS

DEM	Discrete element method
°C	Celsius Degrees
$_i$ and $_j$	Particle *i and j*
IFA	Institute of Occupational Safety and Health of the German Social Accident Insurance
$d_{i,j}$	Distances from the mass centers of particles *i* and *j*
e	Restitution coefficient
E	Young's Module
E_{eff}	Equivalent Young Module
$\vec{F_i}$	Full-Force vector
Fr	Froude number
F_N	Normal Force
F_T	Tangential Force
g	Gravity
G	Shear module
G_{eff}	Equivalent shear module
Hz	Hertz
LAMMPS	Large-scale Atomic/Molecular Massively Parallel Simulator
LIGGGHTS®	LAMMPS improved for general granular and granular heat transfer simulations.
M	meters
m_i e m_j	Mass of particles *i* and *j*
m^*	Equivalent mass
PLA	Polylactic acid polymer
RPM or rpm	Revolutions per minute
R or *r*	Radius
R_i and R_j	Particle radius *i* and *j*
R_{min}	The radius of the smallest particle
R_{eff}	Effective radius
S_N	Normal stiffness
S_T	Tangential stiffness
t_R	Rayleigh wave (time)
v_{ret}	Return speed
v_{imp}	Impact speed
UFPR	Federal University of Paraná
W	Watts

$\overrightarrow{F_{ij}^{C}}$	The contact force between particles *i* and *j*
$\overrightarrow{F_{ij}^{N}}$	The contact force between particles *i and j in* the normal direction
$\overrightarrow{F_{ij}^{T}}$	The contact force between particles *i and j in the* tangential direction
$\overrightarrow{F_{i}}$	Total forces vector
$\overrightarrow{M_{i}}$	Total torque vector
$\overrightarrow{M_{ij}^{t}}$	Rotational torque vector
$\overrightarrow{M_{ij}^{r}}$	Torque on rolling resistance
$\overrightarrow{n_{ij}}$	Unit vector from particle i to j
$v_N^{\overrightarrow{rel}}$	Relative speed in the normal direction
$v_T^{\overrightarrow{rel}}$	Relative speed in the tangential direction
$\vec{V}_i$ and $\vec{V}_j$	Speed vector in direction *i* and *j*
$\vec{x}_i$ and $\vec{x}_j$	Position vector in direction *i* and *j*

Greek symbols

β	Damping coefficient
δ	Overlap
δ_N	Normal overlap
δ_T	Tangential overlap
ω	Angular velocity
ω_i	Angular velocity of particle *i*
$\vec{\omega}_i$	Angular velocity vector particle *i*
$\vec{\omega}_j$	Angular velocity vector particle *j*
ω_c	Critical angular velocity
μ	Static coefficient of friction
μ_R	Rolling friction coefficient
μm	Micrometer
υ	Poisson coefficient
ρ	Particle density
2D	Two Dimensions
3D	Three Dimensions

SUMMARY

1. INTRODUCTION

Granular materials are used in the chemical, pharmaceutical, food, beverages, metallurgical, fertilizer, and mineral industries, among others. Those who focus on improving operational models into more analytical and fast processes. As a result, software and methodologies are being developed to meet this demand. Particulate matter research has only recently developed rapidly in the scientific community. It all started with Cundall and Strack's most significant advancement coming in the 1970s when they presented a consistent approach to the subject.

The discrete elements method (DEM) presents numerous approaches for obtaining an effective granular material modeling technique in which a study of particles is applied in an idealized way by setting the information of the spheres in their entirety and their behavior, when present in packaging. As a result of the refinement of complex models such as particle mixing and segmentation, the use of this model becomes much more appropriate.

Since the DEM is based on a Lagrangian methodology, the approaches of Newton's second law are used to understand the properties of granular flows. Furthermore, particle interactions are described in the normal and tangential directions, with rigid (Hard Contact) or deformable (Soft Contact) characteristics. Besides that, the contacts can be classified as particle-particle (between particles) or particle-wall (a particle with the recipient wall).

Density, particle size, friction coefficients, and equipment geometry, among other factors, have a significant impact on the achievement of operating regimes as well as the final behavior of particle packing. The simulation process, via LIGGGHTS®, aims to provide a real-time reproduction of particle studies that are faster and more predictive of their behavior. When reproducing practical experiments in simulations, it is critical to use the correct parameters, for example, the ones cited above. Obtaining the data for the simulation is not always straightforward, which necessitates calibration.

The food sector employs a wide range of granular inputs, from "raw" products to industrial. Because of their large product line, they hardly provide a complete analysis of their physical attributes in the literature.

Sugar is a crucial constituent in the Brazilian food sector. There are currently various varieties, including granulated, refined, inverted, demerara, and others; nevertheless, there have been few investigations on their qualities, such as friction coefficients. They are critical in establishing optimal processing conditions for this "raw" material, such as the mixing process.

1.1. OBJECTIVES

The purpose of this master's dissertation is to investigate the structure of the DEM theory, operational regimes in rotating drums, and the effects of friction coefficients, to develop a descriptive system for reproducing the experimental part in LIGGGHTS® software. As a result, it attempts to qualify the used model as well as define the parameters studied for crystal sugar. In this regard, the following strategic targets are proposed:

- Reproduction of a practical experiment from the literature in software for testing the ability to describe experimental data in LIGGGHTS®.
- Validate the suggested model using literature-reviewed data from the Benchmarking Study.
- To determine the static and rolling friction coefficients between particles that describe the behavior of particles in a rotating drum by simulation.
- To compare the simulation results with experimental data.

2. BIBLIOGRAPHIC REVIEW

It presents the literature review on DEM (2.1), a systemic view of DEM (2.2), contact models and mechanisms, respectively (2.3 and 2.4), and a numerical approach (2.5). Also describes a review of particulate materials (2.6), the main parameters used for analysis and simulation (2.7), and a review about LIGGGHTS® (2.8).

2.1. DISCRETE ELEMENT METHOD (DEM): AN OVERVIEW

The DEM (Discrete Element Method) is a numerical technique with effective modeling in the analysis of granular materials (GOMES, 2014; O'SULLIVAN, 2011; NOROUZI *et. al.,* 2016). DEM uses a set of information, including discrete geometry, theoretical physics, and the representation of numerical computation (HABIB *et. al.,* 2014 *apud.* WASSGREN 1997; FAZEKAS, 2007).

The concept of simulation is based on the individual consideration of particles; the analytic process allows for an idealized study of them (GOMES, 2014; O'SULLIVAN, 2011; NOROUZI *et. al.*, 2016). Granules in DEM are generally considered to be solid particles; their mechanical behavior is usually not linear (GOMES, 2014; NOROUZI *et. al.*, 2016).

The development of DEM came mainly from issues involving engineering and geological approaches. Several investigations were initiated between 1970 and 1989 for concepts driven by the study of soil processes and particle mobility and deformation. Cundall and Strack, on the other hand, reported the development of a more sophisticated methodology, now known as the discrete element method, in the 1970s (JING and STEPHANSSON, 2007). More solid proportions on DEM were established in 1979, and Cundall and Strack investigated the two most common approaches to particles: soft particles and hard particles (ZHU *et. al.,* 2007).

DEM is used in a wide range of areas, including chemical and civil engineering, geomechanics, pharmaceuticals, grain storage and processing, mining, and thus more (GOMES, 2014; O'SULLIVAN, 2011; ABI-MANSOUR, 2019). The ability to simulate granular systems using DEM is correlated to the simplification of complex models such as particle transport, mixing, and segmentation processes (HABIB *et. al.,* 2014 *apud.* ASMAR *et. al.,* 2002, FRAIGE and LANGSTON, 2006, ZHU *et. al.,* 2008).

2.2. A SYSTEMIC VIEW OF THE DEM

DEM is related to a Lagrangian approximation, which employs Newton's second law approach to describe the properties of granular flows (BRANDÃO, 2017; SAKAI *et. al.,* 2012). The contact calculations are performed by using particles' coordinates and radius, which are determined by the system's interactions (O'SULLIVAN, 2011; NOROUZI *et. al.*, 2016). Figure 1 illustrates the process of particle-wall and particle interaction, the delta (δ) is referred to as the elements overlap.

Figure 1 - Particle-Particle and Particle-Wall Contact

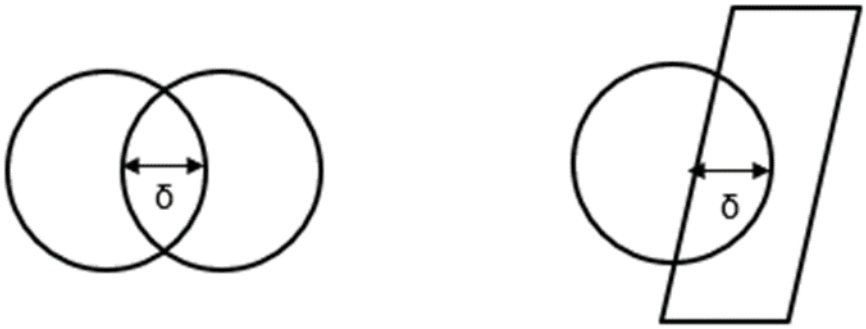

Source: Adapted from Peng, 2014.

When contact occurs, the impacts are investigated in both normal and tangential directions. The tangential force is considered to be zero in cases when there is no friction, *i.e.* when the bodies slide without resistance. In this method, the contact's description is entirely focused on the normal force (SAMPAIO, 2017). Newton's first law, on the other hand, appears to be true when no force is acting on the particle, so the body will maintain its initial state and the linear and angular velocity variables will remain unaffected (CAMPOS, 2016).

The DEM algorithm treats each particle's dynamic increment as a discrete increment of time (O'SULLIVAN, 2011). Particles can accept 2D and 3D geometric shapes as well as more complex shapes including polygonal, polyhedral, or cubic (O'SULLIVAN, 2011; HABIB *et. al.,* 2014 *apud.* FRAIGE *et al.*, 2008).

In summary, the DEM calculation system is composed of three procedures: contact detection, force calculation, and particle position increment for the next interaction. In a simple term, simulation is associated with the initial identification of the positions and velocities of the particles, which leads to the determination of the contacts (normal and tangential overlaps), as well as the verification of the forces

involved and the acceleration. In this way, the calculation cycle starts again (SAMPAIO, 2017).

2.3. CONTACT MODELS

Each type of material has its own set of characteristics, although they must be examined in each case study. Several factors can impact the particles, which can be influenced in an isolated way or not in the analysis, leading to more complex problems for the results. These situations include temperature range, material properties (such as roughness), and possible changes in geometry caused by mechanical contact (SAMPAIO, 2017). The contact models follow a classification according to their characteristics The particle interaction may be separated into a macro and micro perspective of the system. The first depicts a divide based on how the contacts occur: whether they are effectively present contacts (elastic or inelastic) or not (non-contact). In the micro view, it can be seen how they take place and what models are used in each situation (elastic or inelastic contact and non-contact). The phenomena and models presented in Figure 2 will be discussed in detail across the sections.

Figure 2 - Classification of interaction forces (contact and non-contact).

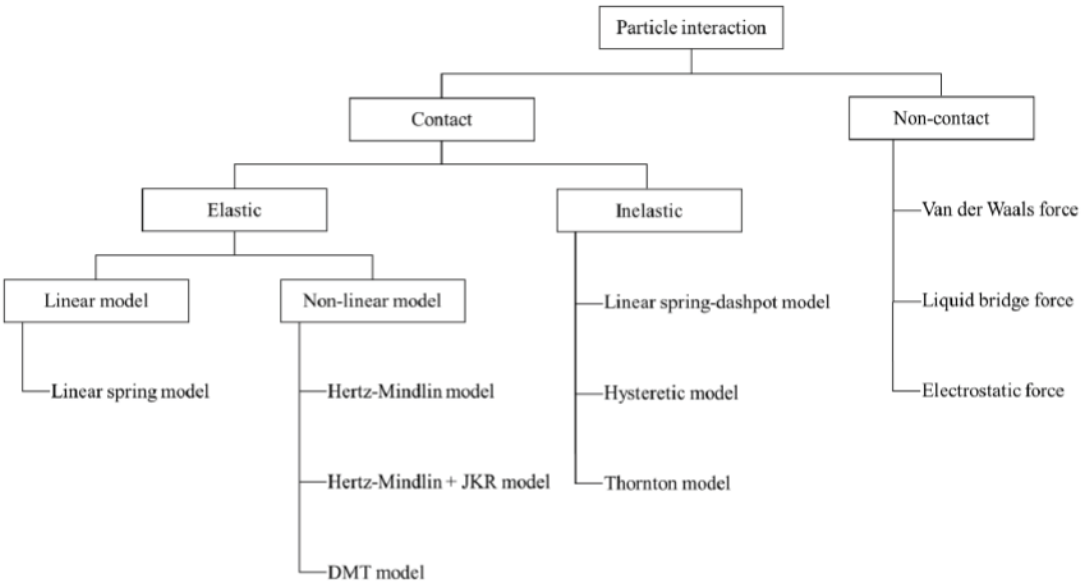

Source: YEOM *et. al.,* 2019.

External forces, such as electrostatics and fluids, have a direct impact on the DEM, making particle mass and density meaningful for simulation (HABIB *et. al.*, 2014 *apud*. WASSGREN, 1997). Cohesive and adhesive forces are essential in the study of granular materials. Among them are the drag force, van der Waals force, liquid bridge,

viscous, and capillaries (see 2.5.4 section). Cohesion forces, for example, are associated with non-contact, which includes van der Waals forces, and adhesives are related to wet materials (JASEVIČIUS *et. al.,* 2017; LU *et. al.,* 2019; TANG *et. al.,* 2019; ENDRES, 2021).

2.4. CONTACT MECHANISMS

Particle interactions can be rigid (Hard Contact or Hard Sphere) or deformable (Soft Contact or Soft Sphere); this method has two analysis groups (CUNDALL and HART, 1992; NOROUZI, *et. al.*, 2016). In general, it is assumed that in "soft contact," the particles with deformable characteristics allow for particle overlap. The particles are rigid in hard contact, which indicates there is no overlap between them (CUNDALL and HART, 1992).

The conditions mentioned in the previous section should not be chosen randomly. The type of contact must be chosen based on physical principles rather than the associated numerical facility (CUNDALL and HART, 1992).

2.4.1. Soft Contact

In soft contact, a limited fraction of overlap is allowed, such an assertion can be comparable to the deformation that the particles undergo (O'SULLIVAN, 2011). Figure 3 illustrates a diagram of the dynamics of this model, the particles collide with an initial velocity, the overlapping occurs, and they move away with different velocities than the original one. Another principle of this approach is the overlaps that occur between particles are much smaller compared to their size (NOROUZI *et. al.*, 2016).

Newton's equation of motion is used in this approach so that at each iteration, a new value corresponding to the positions and velocities of the particles is obtained. The integration varies to the collision time is constant and relatively small at each step (SAMUI *et. al.,* 2016). As an outcome, the contact time interval between the bodies enables more iteration. In other words, it allows a particle to have more than one contact with the others at a time (NOROUZI *et. al.,* 2016).

Figure 3 - Soft Contact Schematic

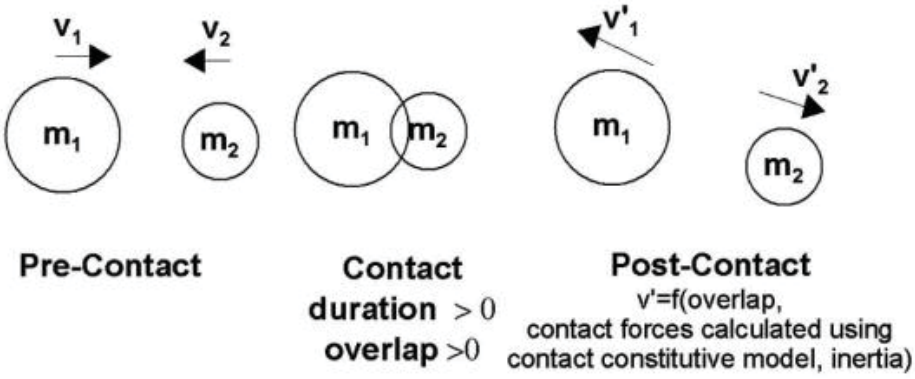

Source: O' Sullivan, 2011.

2.4.2. Hard Contact

At first, hard contact implies that the bodies have no overlap. Furthermore, the contacts are presumed to have a short duration so that the moment changes can be modeled and calculated by the energy loss in the collision (CUNDALL and HART, 1992; O'SULLIVAN, 2011). Figure 4 illustrates a diagram of the dynamics of this model, particles collide at an initial velocity, there is no overlapping, and they go away at different velocities than the original.

The presentation of diluted systems with low density is associated with a good description of the Hard Contact model. Collisions are more common although the duration of contact between the bodies is short. Particles in systems can move freely, influenced by external forces and translational speeds (NOROUZI *et. al.*, 2016).

Figure 4 - Hard Contact Schematic

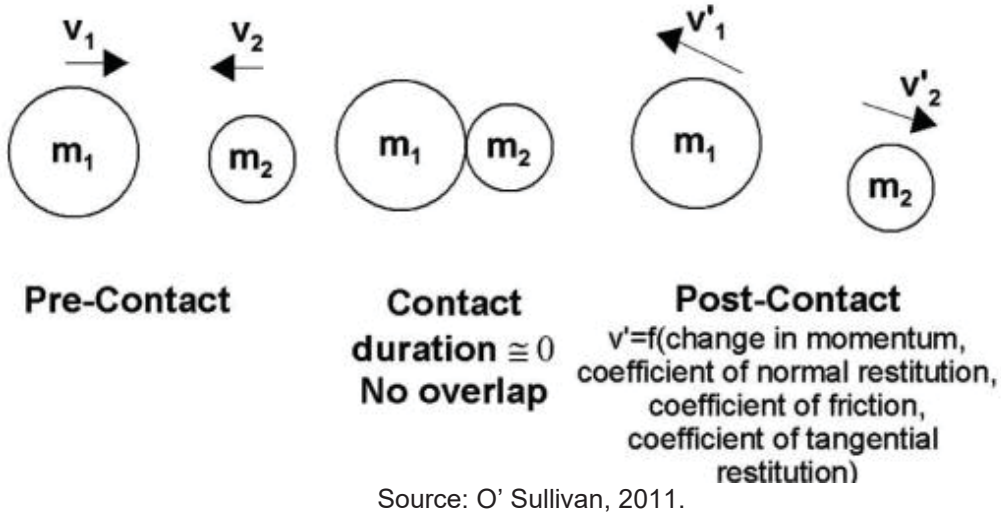

Source: O' Sullivan, 2011.

2.5. NUMERICAL APPROACH

One of the primary distinctions between the soft contact and hard contact approaches is that the mathematical purpose for the deformable sphere is in differential form. Another consideration is that in this system, information about forces and torques must be obtained at each interval, so each increment of time is assumed to be small. Thus, the disturbances of the contacts only allow them to propagate in the particles around each other, so between every increment, the solution for multiple contacts can be measured directly to a single particle (CAMPOS, 2016).

The precise determination of the method's accuracy is critical for a decent system simulation. As the variations in time between each step are generally small, certain factors, such as the forces and accelerations of the particles that act in a constant manner and their velocities that change linearly, must be considered (HABIB *et. al.*, 2014 *apud.* ASMAR *et. al.*, 2002, FRAIGE and LANGSTON, 2006).

Acknowledging each variable's implied meaning in the process analysis is an effective way of identifying the dynamics of particle motion. Figure 5 shows a typical model of two particles colliding (three-dimensional), each component of the motion dynamics is related, as described the vectors $\vec{x}_i$ and $\vec{x}_j$ describing the positions of the mass centers, the velocity vectors $\vec{V}_i$ and $\vec{V}_j$, angular velocity vectors $\vec{\omega}_i$ and $\vec{\omega}_j$, the sub-indices *i* and *j* representing the particles, respectively (NOROUZI *et. al.*, 2016; IDAGAWA, 2017).

Figure 5 - Simplified contact scheme.

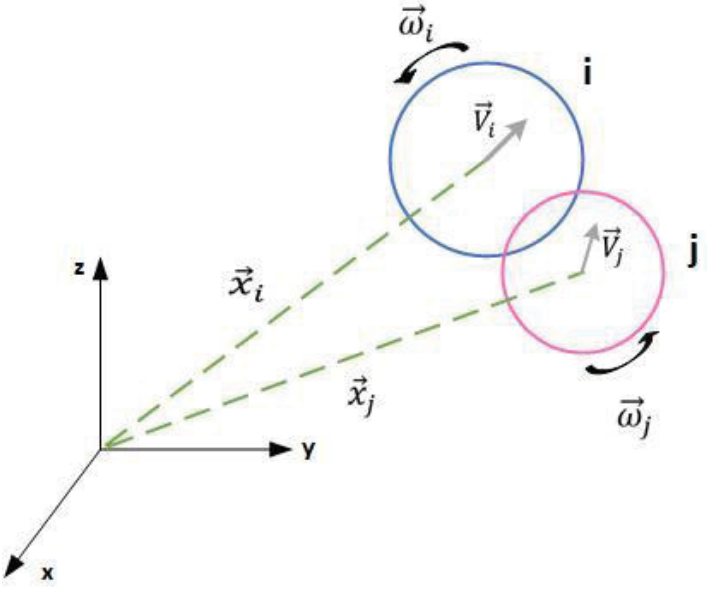

Source: Adapted from Norouzi, *et. al.*, 2016.

Two laws can be used to represent the motion equations of spherical particles; it is important to note that rolling is a combination of rotational movements and pure translation (HALLIDAY, 2018; NOROUZI *et. al.*, 2016). The law of motion, as described by Newton's second law, is responsible for the process of particle translation, and Euler's second law of motion is rotation, which takes into account the centers of mass of each of the bodies. The mathematical description is based on equations (1) and (2), which represent the total torque ($\overrightarrow{M_{\mathrm{i}}}$) and the sum of all forces ($\overrightarrow{F_{\mathrm{i}}}$) (NOROUZI *et. al.*, 2016).

$$m_{\mathrm{i}} \cdot \frac{d\overrightarrow{V_{\mathrm{i}}}}{dt} = m_{\mathrm{i}} \cdot \frac{d^2\overrightarrow{x_{\mathrm{i}}}}{dt^2} = \overrightarrow{F_{\mathrm{i}}} \tag{1}$$

$$I_{\mathrm{i}} \cdot \frac{d\overrightarrow{\omega_{\mathrm{i}}}}{dt} = I_{\mathrm{i}} \cdot \frac{d^2\overrightarrow{\varphi_{\mathrm{i}}}}{dt^2} = \overrightarrow{M_{\mathrm{i}}} \tag{2}$$

The analysis requires numerical solutions. In this way, the interactions are used to carry out the computation of the DEM simulation. First, the interaction forces of the particles are calculated, and then the equations of movement are integrated to obtain a new combination of data. Equations (3) and (4) are mostly destined for DEM simulations (NOROUZI *et. al.*, 2016; IDAGAWA, 2017).

$$m_{\mathrm{i}} \cdot \frac{d\overrightarrow{V_{\mathrm{i}}}}{dt} = m_{\mathrm{i}} \cdot \frac{d^2\overrightarrow{x_{\mathrm{i}}}}{dt^2} = \sum_{j=1, j\neq \mathrm{i}}^{n} \overrightarrow{F_{\mathrm{ij}}^{p-p}} + \overrightarrow{F_{\mathrm{i}}^{p-f}} + \overrightarrow{F_{\mathrm{i}}^{ext}} \tag{3}$$

$$I_{\mathrm{i}} \cdot \frac{d\overrightarrow{\omega_{\mathrm{i}}}}{dt} = I_{\mathrm{i}} \cdot \frac{d^2\overrightarrow{\varphi_{\mathrm{i}}}}{dt^2} = \sum_{j=1, j\neq \mathrm{i}}^{n} \left(\overrightarrow{M_{\mathrm{ij}}^{t}} + \overrightarrow{M_{\mathrm{ij}}^{r}}\right) \tag{4}$$

Where:

- *p-p* (particle - particle): representation of the collision forces of the particles.
- *p-f* (particle – fluid): forces working on the particle due to fluid.
- *ext* (external forces): forces from uniform or non-uniform field as gravitational or electromagnetic force.
- $\overrightarrow{M_{\mathrm{ij}}^{t}}$ (tangential torque): responsible for generating the rotations in the particles.
- $\overrightarrow{M_{\mathrm{ij}}^{r}}$ (torque on rolling resistance): friction between the particles causes movement in the opposite direction.

Whenever a particle is exposed to one or more simultaneous collisions, a process of overlap occurs between them, called normal overlap (δ_N). The smallest condition for a contact between the bodies is $\delta_N > 0$, where $\overrightarrow{x_i}$ and $\overrightarrow{x_j}$ are position vectors and R_i and R_j the radius, and the indices *i* and *j* represent the particles, respectively (NOROUZI *et. al.*, 2016). The mathematical relationship for normal overlap between spheres is presented in Equation (5). The magnitude of this overlap depends on the relative position, dimension, particle shape, and perpendicular orientation of particles on the surface (FAZEKAS, 2007).

$$\delta_N = R_i + R_j - \left|\overrightarrow{x_j} - \overrightarrow{x_i}\right| \quad (5)$$

2.5.1. Contact force model

The non-continuous force-displacement model, which describes a more realistic model of granular flows and has a greater application in simulation processes. Physical contact between two particles is calculated using the force-displacement law, which considers some collision properties (NOROUZI *et. al.,* 2016):

- Normal and tangential overlaps.
- Physical characteristics.
- Contact collisions in the past.

Figure 6 - Scheme of the collision system between two particles.

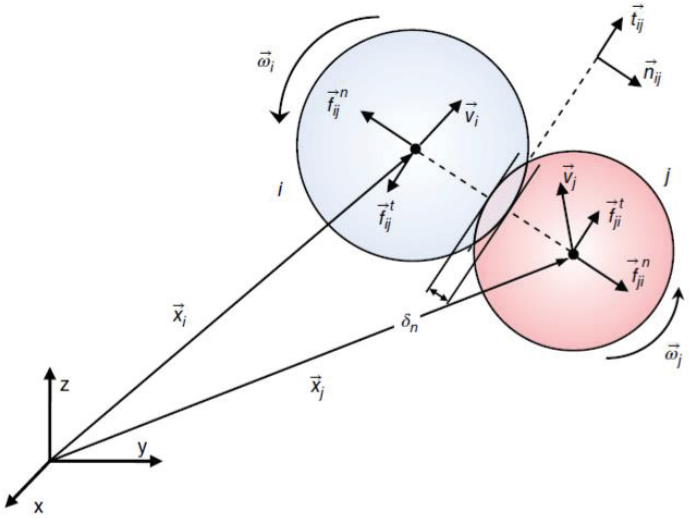

Source: Norouzi *et. al.,* 2016.

The contact force ($\overrightarrow{F_{ij}^{C}}$) between the particles is decomposed into two components, as shown in Figure 6 represents the contact between two particles,

indicating the influencing vectors in the dynamics of the movement, which are normal ($\overrightarrow{F_{ij}^{N}}$) and tangential ($\overrightarrow{F_{ij}^{T}}$). As a result, equation (6) describes the contact force (NOROUZI *et. al.*, 2016; IDAGAWA, 2017; ASMAR *et. al.,* 2002):

$$\overrightarrow{F_{ij}^{C}} = \overrightarrow{F_{ij}^{N}} + \overrightarrow{F_{ij}^{T}} \quad (6)$$

2.5.1.1. Hertz – Mindlin Contact Models

It is a nonlinear viscoelastic model that exhibits a relationship between normal force and displacement, as well as more representative accuracy in the calculation of particle collision forces. Heinrich Hertz (1882) proposed the behavior of particle collision in the normal direction first, and later included the portion responsible for particle adhesion. Mindlin and Deresiewicz developed the theory of tangential elastic contact between particles (NOROUZI *et. al.,* 2016; YEOM *et. al.,* 2019).

The models presented according to Hertz-Mindlin's theory do not present slippage (PENG, 2014; YEOM *et. al.,* 2019). Equation (7) determines the Hertzian contact model for an elastic contact between particle-particle and particle-wall in the normal direction, where *E* expresses the Young module, δ characterized by particle overlap, υ Poisson coefficient, and subscripts *i* and *j* represent their respective particles (JASEVIČIUSA *et. al.,* 2017; Li *et. al.,* 2009; NOROUZI *et. al.,* 2016; PARAB *et. al.,* 2017; TORBAHN *et. al.,* 2017). The contact force expressed by Equation (8), Coulomb's friction law must be respected $F_T \leq \mu \,.\, F_N$, μ defined as consisting of the static friction coefficient, which is associated with a significant influence on the displacements in the tangential direction, being G_{eff} the equivalent shear module (PENG, 2014; HEILBUTH, 2017). The Young modulus is related to the material's elastic deformation and the shear modulus (HESSEL *et. al.,* 2016). Poisson's ratio refers to the connection between lateral and axial strain in elastic strain. The shear modulus, on the other hand, analyzes the element's deformation (TIMOSHENKO and GERE, 1983).

$$F_N = \frac{4}{3} \,.\, E_{eff} \,.\, \sqrt{R_{eff}} \,.\, \delta_N^{3/2} \quad (7)$$

$$F_T = -8\, G_{eff} \,.\, \sqrt{R_{eff} \,.\, \delta_N} \,.\, \delta_T \quad (8)$$

$$\frac{1}{R_{eff}} = \frac{1}{R_1} + \frac{1}{R_2} \quad (9)$$

$$\frac{1}{E_{eff}} = \frac{1 - v_i^2}{E_i} + \frac{1 - v_j^2}{E_j} \quad (10)$$

$$\frac{1}{G_{eff}} = \frac{2 - v_i}{E_i} + \frac{2 - v_j}{E_j} \quad (11)$$

Figure 7 shows that the normal contact force increases as the overlap (δ) between the particles increases, reaching its maximum value when their centers overlap (PENG, 2014; YEOM *et. al.,* 2019).

Figure 7 – Contact force and displacement: Hertz-Mindlin.

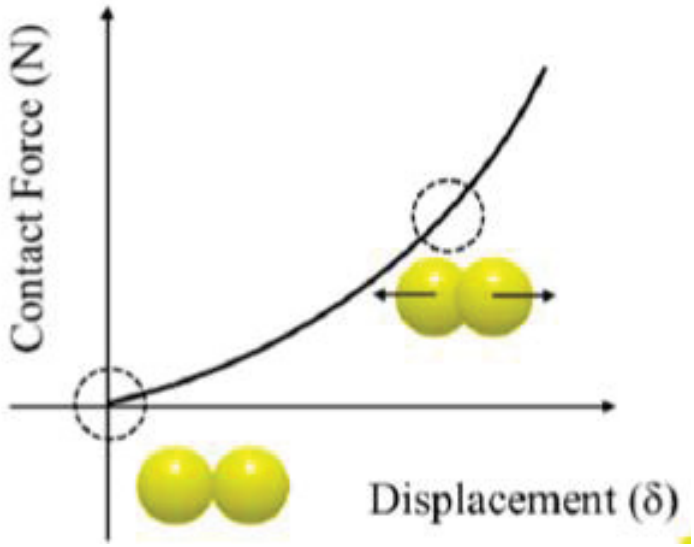

Source: YEOM *et. al.,* 2019.

They present the same elastic force principle, but the dissipative component, the viscous force, is included in the total computation of normal direction data (NOROUZI *et. al.,* 2016). The normal force, which is correlated with damping (viscous force), can be described in Equation (12) and tangentially in Equation (13) where, e restitution coefficient, β damping coefficient (related to the restitution coefficient) (14), S_N is the normal stiffness (15) and S_T the tangential stiffness (16), m^* is equivalent mass (17), $v_N^{\overrightarrow{rel}}$ relative speed in normal and $v_T^{\overrightarrow{rel}}$ tangential directions (HEILBUTH, 2017; ZHOU *et. al.,* 2002; QI *et. al.,* 2017; TAN *et. al.,* 2019).

$$F_N^d = -2 \cdot \sqrt{\frac{5}{6}} \cdot \beta \cdot \sqrt{S_N \cdot m^*} \cdot v_N^{\overrightarrow{rel}} \quad (12)$$

$$F_T^d = -2 \cdot \sqrt{\frac{5}{6}} \cdot \beta \cdot \sqrt{S_T \cdot m^*} \cdot \overrightarrow{v_T^{rel}} \quad (13)$$

$$\beta = -\frac{\ln e}{\sqrt{\ln^2 e}} \quad (14)$$

$$S_N = 2 \cdot E_{eff} \cdot \sqrt{R_{eff} \cdot \delta_N} \quad (15)$$

$$S_T = 8\, G_{eff} \cdot \sqrt{R_{eff} \cdot \delta_N} \quad (16)$$

$$m^* = \frac{m_1 \cdot m_i}{m_i + m_1} \quad (17)$$

Several models were proposed for the dissipative part in the normal direction, such as the Kuwabara and Kono model (KKn) and the Tsuji, Tanaka, and Ishida model (TTIn) (NOROUZI *et. al.,* 2016).

2.5.2. Particle torque model

The shear responsible for particle torque is essentially the sum of two components: the one responsible for rotational torque and the one responsible for rolling resistance. The particle's rotational torque, equation (18), is caused by a tangential contact that makes the body "rotate" (NOROUZI *et. al.*, 2016). Where, M_{ij}^t is tangential torque, R_{i} radius of particle *i*, $\overrightarrow{n_{\mathrm{ij}}}$ unit vector from particle *i* to *j*, $\overrightarrow{F_{\mathrm{ij}}^C}$ contact force particles *i* and *j.*

$$\overrightarrow{M_{\mathrm{ij}}^t} = R_{\mathrm{i}} \cdot \overrightarrow{n_{\mathrm{ij}}} \times \overrightarrow{F_{\mathrm{ij}}^C} \quad (18)$$

To explain this phenomenon, several models have been developed (NOROUZI *et. al.,* 2016). The torque of the contact surface is defined by the Hertz-Mindlin model, Equation (19) or can be expressed by Equation (20), which represents the μ_R coefficient of rolling friction, F_N the normal contact force, $d_{i,j}$ the distances between the mass centers of particles *i* and *j*, and ω_i the angular velocity of particle *i* and R_{eff} effective radius (ENDRES *et. al.,* 2021 *apud.* SCHILDE *et. al.,* 2014; NOROUZI *et. al.,* 2016; TAN *et. al.,* 2019).

$$\tau_i = -\mu_R . F_N . d_{i,j} . \omega_i \quad (19)$$

$$\overrightarrow{M_{ij}^{r}} = -\mu_R . R_{eff} . \left|\overrightarrow{F_{i,j}^{N}}\right| . \left(\frac{\vec{\omega}_i - \vec{\omega}_j}{\left|\vec{\omega}_i - \vec{\omega}_j\right|}\right) \quad (20)$$

2.5.3. Particle-Wall Contact Force

Correlated interactions between particles and the vessel wall can be modeled similarly to particle contact. In this case, the interaction uses constant values that are appropriately applied to the particle-wall interaction (ASMAR *et. al.,* 2002).

The contact of particles with corners of the wall (for example, contacts between two walls) can only be listed once for the simulation; this is a limitation of the model. In simulations, the significance of this particle-wall correlation is lower than that of particle-particle (ASMAR *et. al.,* 2002; HABIB *et. al.,* 2014).

2.5.4. Non-contact forces

The van der Waals force is one of the main forces of interaction between particles with a 100 nm spacing between them (LU *et. al.,* 2019). It has been notable for exhibiting dipole-dipole, dipole-induced, and dipole-instantaneous attractive forces (YEOM *et. al.,* 2019). The representative model of strength for fine particle/ultrafine systems is provided by Hamaker (the most used model), but in some studies, models can be based on Lifshitz's theory (LU *et. al.,* 2019; YEOM *et. al.,* 2019). For particles with diameters greater than 30 μm, this force is usually omitted (PARTELI *et. al.,* 2014).

The liquid bridge force is composed of a capillary force and a viscous force that considers wet particle systems (TANG *et. al.,* 2019). If the relative humidity of the system is less than 40%, this force can be ignored (PARTELI *et. al.,* 2014). When the liquid viscosity or relative velocity in the system exceeds the normal value, viscous forces become significant (TANG *et. al.,* 2019). Capillary bridges exist in systems where a significant portion of the particles are moist (ENDRES *et. al.,* 2021 *apud.* ANTONYUK, PALIS, and HEINRICH, 2011, TSUNAZAWA, FUJIHASHI, FUKUI, SAKAI and TOKORO, 2016). They are linked to the system's humidity; if it remains below 50%, the force will not contribute to the interactions (JASEVIČIUS *et. al.,* 2017 *apud.* ZENG, MARTIN, and MARRIOTT, 2001).

Hydrodynamic interactions are related to drag forces. It is critical in simulations for the analysis of particle-fluid flows (NOROUZI *et. al.*, 2016) Stokes' law of drag is valid in laminar flow regimes with Reynolds numbers less than one (MAXWELL *et. al.,* 2010; MORENO-ATANASIO, 2013).

Electrostatic forces are associated with attractive and repulsive forces between particles. This is a common phenomenon in situations where isolated particles fluidize. Coulomb's law expresses this non-contact force, which can have a significant impact on the gas-solid hydrodynamic process (TAN *et. al.,* 2019).

2.5.5. Rayleigh waves

The simulation's particle movements involve multiple contacts, resulting in high demand for interaction calculations (HEILBUTH, 2017). The Rayleigh wave, shown in Figure 8, is a mechanical wave that travels across the surface of the particles, and it is intended to use a wave value for the system's smallest sphere (BRANDÃO, 2017 *apud.* DANBY *et. al.* 2013).

Figure 8 – Rayleigh waves.

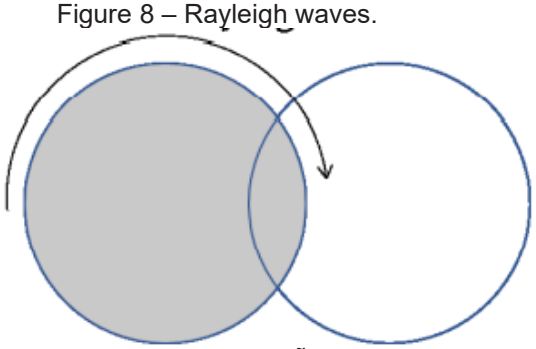

Source: BRANDÃO, 2017.

The time of Rayleigh is given by equation (21), where R_{min} is the radius of the smallest particle in the set, ρ is the particle density, υ is the Poisson ratio, and G is the shear module, considering isotropic materials (HEILBUTH, 2017; LI *et. al.,* 2009; MARIGO *et. al.,* 2015; GARCIA, 2010). As a result, given the smallest particle in the system, the mentioned step must be smaller than the Rayleigh wave (HEILBUTH, 2017 *apud.* THAKUR, 2014).

$$t_R = \frac{\pi \,.\, R_{min}}{0{,}8766 + 0{,}163 \,.\, \upsilon} \cdot \sqrt{\frac{\rho}{G}} \tag{21}$$

$$\upsilon = \frac{E}{2 \,.\, G} - 1 \tag{22}$$

The enumerated step must be small enough so that the wave does not spread beyond the particle contact centers (NOROUZI *et. al.*, 2016). The chosen value requires stability in the integration time, which ought to be less than the suggestion of applying the 20% (high particle densities) to 40% (low particle densities) of the value given by equation (21) (HEILBUTH, 2017 *apud.* EDEM, 2011; MARIGO *et. al.,* 2015); on the other hand, the step can be established as 10% of Rayleigh's time (YARI *et. al.,* 2020).

2.6. PARTICULATE MATERIALS

Particulate materials are frequently used in rotating drums in chemical, pharmaceutical, metallurgical, fertilizer, minerals, and other industries. However, there are some difficulties in obtaining data in these procedures, such as particle collision factors and particle-particle and particle-wall interactions (SONI *et. al.,* 2016; XU *et. al.,* 2010).

2.6.1. Parameters for particle analysis in rotating drums

The dynamics of particles present in rotation equipment frequently do not allow for simple parameter prediction. The volume of particles, the size and shape of the container, and the speed of rotation are macroscopic parameters; particle size, density, and roughness are microscopic parameters (AYENI *et. al.,* 2015). Mixing processing of granular materials is generally done in cylindrical drums, where in their axial direction, rotation applies. The particles in this system construct a kind of "bed" that can have a static or dynamic repose angle; this characteristic is related to the system's rotational speed (DAVIDSON *et. al.,* 2000). The main macroscopic forces present in the rotating drum are centrifugal and gravitational forces (AYENI *et. al.,* 2015). Particle displacement in the drum is influenced by normal and tangential forces, friction, and particle weight; random collisions occur during the mixing process; and a single particle cannot move freely without colliding with another (XU *et. al.,* 2010).

The drum operating regime is closely associated with the number of Froude, which is correlated with the angular speed of operation of the system. Despite being an excellent parameter for the investigation of the drum operating regime, each material presents its singularities (BOATENG, 2016; DAVIDSON *et. al.,* 2000).

The number of Froude has a correlation with centrifugal and gravitational forces, as shown by their ratio (23), where *n* is the frequency of rotation, R is the radius of the drum, and g is gravity (KOMOSSA *et. al.,* 2014). In addition, if you consider it in the range of $10^{-4} < Fr < 10^{-2}$, the dominance of gravitational force over the centrifuge stands out (AYENI *et. al.,* 2015).

$$Fr = \frac{\left(2 \,.\, \pi \,.\, n/_{60}\right)^2 . R}{g} \tag{23}$$

For the operation regimes, six possible types are considered in Figure 9, which are slipping, slumping, rolling, cascading, cataracting, and centrifuging (AYENI *et. al.,* 2015; XU *et. al.,* 2010; HENEIN *et. al.,* 1983).

- In the slipping regime, the particle bed assumes a stationary configuration. With this, they slowly slip to the other end of the drum as its rotation occurs.
- A slumping regime relates to a constant detachment of the particles of the bed, which are directed to the other end of the drum whenever there is a rotational movement, taking it to a higher angle of repose.
- The rolling regime defines a constant movement of particle layers; the rotational velocity is relatively low, the resting angle is constant, and the surface is smooth and flat.
- The cascade regime presents kinetic energy higher than the previous regime, so the particles begin to be driven, reaching the opposite wall of the drum.
- The cataract regime exposes high dynamics, resulting in a greater number of collisions between the particles and the drum.
- The centrifugal regime is characterized by the proximity of the critical speed of rotation.

As shown in Figure 9, increasing the rotation causes the materials inside the drum to enter a more intense regime, resulting in more constant collisions and thus improving the mixing process (XU *et. al.,* 2010). As previously stated, the properties of the mixtures are affected by the rotation speed and can take on a sliding or centrifuge configuration, which is directly related to the repose angle, which is connected to the increase in rotation speed. As a result, this angle grows proportionally to the rotation speed and gets smaller proportionately to the increase in particle size (SONI *et. al.,*

2016). The term responsible for angular velocity (ω), equation (23), has a proportional relationship to the number of Froude; the greater the module, the more intense the drum operation, in other words, the existence of a critical regime will increase. Due to the modes of operation of the drums, characteristics are observed, to maximize a mixing process, the rolling regime becomes indispensable for the system, forming two regions: the active and passive layer. The active layer, the main responsible for the mixing process, usually presents itself with a smaller thickness; eventually, there is a need to make this region larger, and the speed of the drum needs to be high, which also manifests a lower restriction to movement, as a result, the particles move with a lower degree of restriction (BOATENG, 2016).

Figure 9 - Operating regimes.

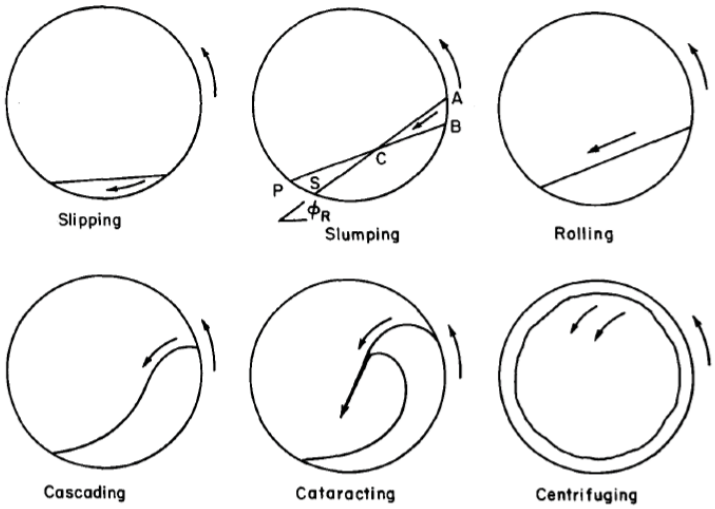

Source: HENEIN *et. al.,* 1983.

2.7. PARAMETERS IN DEM

In the DEM, a few pairs of special analyses are usually required in their simulations, so this section presents a more detailed study of some relevant points.

2.7.1. Young modulus

Young's modulus is defined as the ratio of the material's strain and stress (KADKHODAIE, A. and KADKHODAIE, R., 2022, MA *et. al.,* 2016).

This parameter is related to the basic properties of materials, i.e., as defined by their microstructures and chemical composition. It is defined by the equation (24), as

a result of σ is the material stress and ε is the strain of the material (CARLI *et. al.,* 2018).

$$E = \frac{\sigma}{\varepsilon} \tag{24}$$

2.7.2. Poisson ratio

It is a dimensionless metric defined by the transversal to longitudinal strain ratio (KADKHODAIE, A. and KADKHODAIE, R., 2022). Since it is a homogeneous and isotropic material, the following equation (25) may be used. Considering ϵ_x and ϵ_y the transversal strain and ϵ_z as the longitudinal strain (CARLI *et. al.,* 2018).

$$\upsilon = -\frac{\epsilon_x}{\epsilon_z} = -\frac{\epsilon_y}{\epsilon_z} \tag{25}$$

2.7.3. Restitution Coefficient

The restitution coefficient, Equation (26), is associated with a kinetic energy that is conserved after a particle collision process, as indicated by the return velocity ratio to the impact velocity (FAZEKAS, 2007; HEILBUTH, 2017).

$$\varepsilon = \frac{v_{ret}}{v_{imp}} \tag{26}$$

The restitution coefficient has values ranging from 0 to 1, with 0 implying a perfectly inelastic collision and 1 indicating a perfectly elastic collision in which all energy is conserved (HEILBUTH, 2017 *apud.* CROSS,1999). This coefficient can be calculated using the free fall method (HEILBUTH, 2017), as well as the impact experience of a high-speed camera (KOMOSSA, 2014; MARIGO and STITTI, 2015).

In general, the reconstitution value depends largely on the particle and the normal and tangential directions, but they are described with a single value (ASMAR *et. al.,* 2002; SUHR and SIX, 2016).

2.7.4. Friction coefficients

The frictional force is defined as one body's resistance to moving over another (HUTCHINGS and SHIPWAY, 2017). Since this definition of friction coefficients is complex and often difficult to quantify, they are usually expressed in a range of values rather than a single value (MCKENNA; HEARLE; O'HEAR, 2004) Leonardo Da Vinci

was among the first to conduct experiments on this phenomenon and develop the law of the coefficient of friction (μ), which is given by the quotient of the tangential force (*T*) on the normal (*N*) of the object, given by Equation (27) (BERTHIER, 2001):

$$\mu = \frac{T}{N} \tag{27}$$

- **Static friction**:

Static friction is present at the start of the movement, and it is greater than when the object is already moving (kinetic friction). As a result, the maximum static friction force equals the minimum force required to initiate particle movement (f_e). This ratio is determined by the coefficient of the maximum static friction (μ_e) and the normal force (*N*), Equation (28). The slope angle ratio for an inclined plane where particles initiate a slip can be given by Equation (29) (RESNICK and HALLIDAY, 1983).

$$f_e \leq \mu_e . N \tag{28}$$

$$\mu_e = tg\ \theta_e \tag{29}$$

- **Rolling friction:**

In general, the coefficient of rolling friction promotes control of a particle's rotational movement, indicating the particle's resistance to rotational movement (ZHOU, Y., XU, B. and YU, A., 2001). The rotational movement of the particle is reduced as a result of this resistance, which is also frequently influenced by other frictional forces (HOLMES *et. al.,* 2016). The coefficient can be calculated using (30), where β is the maximum angle formed by particle packaging with the surface and μ_r is the rolling friction coefficient calculated (JUN *et. al.,* 2011).

$$\mu_r = tg\ \beta \tag{30}$$

Further than this point, there is a corresponding correction between this coefficient and the package's resting angle, as the amount of rolling friction is proportional to the angle (ZHOU, Y., XU, B. and YU, A., 2001).

2.8. LIGGGHTS®

LIGGGHTS® is an open-source tool for modeling particulate materials with the discrete element approach. It runs simulations using the chosen boundary conditions,

employing Newton's equations of motion. This name stands for LAMMPS improved for general granular and granular heat transfer simulations. Even though LAMMPS was already applied for granular dynamics simulation (classic model), it formed a support basis for LIGGGHTS® to increase the descriptive capacity of granular materials, particularly for industrial applications (CFDEM, 2011 and 2016).

3. CASE STUDY

Rotary drums are used in a wide range of industrial applications, including mixing, grinding, and drying. The materials present in them may adopt different regimes (see section 2.6.1), which are determined by the geometry of the equipment (diameter and length), operating conditions (degree of filling and speed of rotation of the drum), and particle characteristics (size, shape, and coefficients of friction). All the criteria mentioned are extremely important in defining the operating regime (SANTOS *et. al.,* 2016). In this manner, LIGGGHTS® is a key tool to use since it is necessary to carefully examine each aspect of the system.

Understanding particle interactions in the system is critical when submitting particle materials into rotating drums, a common process in the industry. Used the results of the article from Xu *et. al.* (2010) on a mixing drum, and compared it with a script, APPENDIX 1 - Case study script, by reproducing this study via simulation in the LIGGGHTS® software. Table 1 parameters were considered for this article's study.

Table 1 - Article parameters.

Parameters	Value	Parameters	Value
Length (m)	0.064	Density spheres (kg/m³)	2456
Cylinder diameter (m)	0.241	Young Module (Pa)	5.5×10^{10}
Diameter spheres (m)	0.01014	Poisson Ratio	0.25
Coefficient of friction	0.57		

Source: XU *et. al.,* (2010).

Rayleigh's time must be considered because it is responsible for the system's proper operation. As shown in section 2.5.5, the step times used in this study are 1×10^{-6}, as calculated by equations (21) and (22) using the model's specifications of 20% of t_R. Another factor to consider is the restitution coefficient value of 0.67 (ANGUS *et. al.,* 2020; QI *et. al.,* 2017) and the rolling friction coefficient of 0.05. (ZHOU *et. al.,* 2002).

The rotating drum was evaluated under different angular velocities of 20, 40, 60, and 80 rpm, and in this test, the glass spheres were arranged side by side in the drum (initially segregated), containing 1.200 particles in a proportion of 50% of each color, with the same properties.

In the article studies, only the experimental analysis was performed. In this circumstance, a visual comparison of practice (article) and theory (simulation) was carried out. Individual images shown forward represent the instant of time t ≈ 6 s and the operating regime of each angular velocity (20 to 80 rpm).

According to XU *et. al.* (2010), a rolling process is observed for a rotational speed of 20 rpm; as implied by the decrease in the oscillation of the upper and lower angles of the particle bed, contributing to the origin of a dynamic repose angle (average between the upper and lower angles), passive and active regions are present (see section 2.6.1). As shown in Figure 10, a rolling regime with a constant resting angle exists, and the material remains stable within it. Smoother angular velocities often exhibit a gentler regime, leading to a homogeneous process in which particles are frequently distributed in an ordered manner inside the drum, resulting in only a rolling movement of the particles in the active layer (NOROUZI *et. al.*, 2016; HEILBUTH, 2017; SANTOS *et.al.,* 2016; DAVIDSON *et. al.,* 2000). Figure 11 illustrates the simulation of the chosen parameters at 20 rpm, demonstrating that the rolling regime is present in this case.

Figure 10 - Rolling scheme.

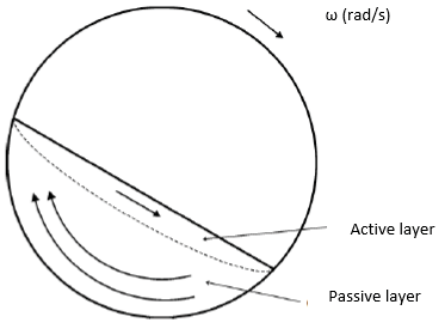

Source: Adapted from Heilbuth, 2017.

Figure 11 - Simulation rolling regime.

Source: The author, 2022.

In the same way, the article (XU *et. al.,* 2010) describes a cascade movement for an angular velocity of 40 rpm. Since the particles have more kinetic energy, they can easily detach from the bed and reach the opposite wall of the drum (Figure 12). This regime is similar to the rolling regime, but the active layer is more visible (NOROUZI *et. al.*, 2016; HEILBUTH, 2017; SANTOS *et. al.,* 2016 *apud.* BLUMBERG and SCHLÜNDER, 1996, MELLMANN, 2001, LIU *et. al.,* 2005, JUAREZ *et. al.,* 2011).

Figure 13 represents the simulation at 40 rpm, and the cascading regime in the drum is seen.

Figure 12 - Cascade scheme.

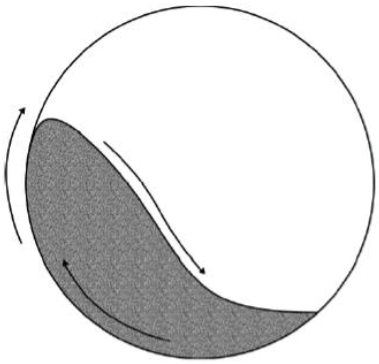

Source: HEILBUTH, 2017.

Figure 13 - Cascade simulation regime.

Source: The author, 2022.

According to the article, by XU *et. al.,* (2010), at 60 rpm, stronger dynamics between the particles occur, resulting in a high rate of collision among them, this is the cataract regime. This property is notorious for increasing angular velocity; as the process begins, the particles are taken to a detachment of the wall from the drum and move through the free space inside the cylinder, colliding with the opposite wall or the particle bed, as shown in Figure 14 (NOROUZI *et. al.*, 2016; HEILBUTH, 2017; BRANDÃO, 2017). Three layers can be seen forming in the drum. The first region contains particles with higher speeds and, as an outcome, a higher launch speed; the second region includes particles that can only roll over the top layer; and the third region consists of the lowest number of spheres and serves as the meeting point for the other regions (NOROUZI *et. al.*, 2016; HEILBUTH, 2017; BRANDÃO, 2017). Figure 15 demonstrates the cataract regime at 60 rpm angular velocity.

Figure 14 - Cataract regimen scheme.

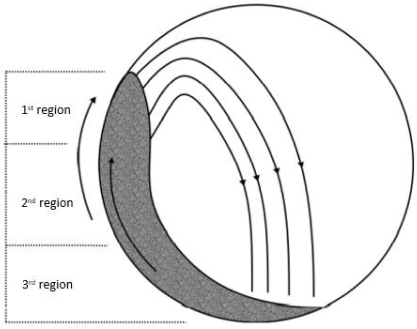

Source: Adapted from HEILBUTH, 2017.

Figure 15 - Cataract simulation regimen.

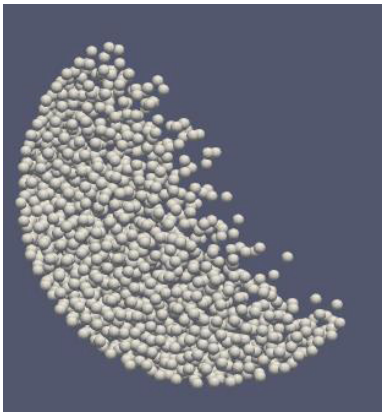

Source: The author, 2022.

According to Xu *et. al.* (2010), 80 rpm is close to a centrifugal regime, but it cannot be considered one. Certainly, because the system is nearing critical velocity, as seen in Equation (31), which in this case is 9,02 s^{-1} according to classical mechanics.

$$\omega_c = \left(\frac{g}{r}\right)^{\frac{1}{2}} \tag{31}$$

The operating regime for the centrifugal regime, Figure 16, changes as the angular velocity increases. The particles that were released are now agglutinated on the drum wall as the process switches from cascading to centrifugation. How the spheres adhere to the wall is related to the number of Froude; as it increases, the particles become closer to the drum wall ($Fr_A < Fr_B < Fr_C$) (NOROUZI *et. al.*, 2016; HEILBUTH, 2017; BRANDÃO, 2017). Figure 17 captures a nearly centrifugal regime at 80 rpm.

Figure 16 - Centrifugation scheme.

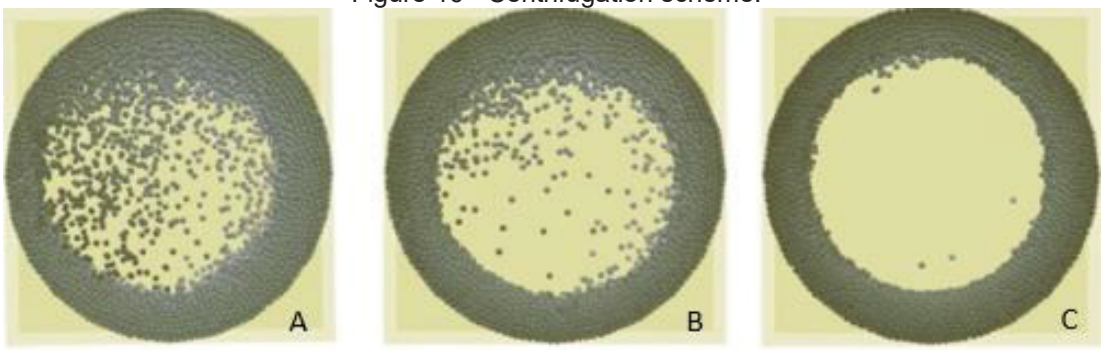

Source: Adapted from NOROUZI *et. al.,* 2016.

Figure 17 - Almost centrifugal simulation regimen.

Source: The author, 2022.

The classification of the operating regime is dependent on each type of material, so the comparison regime *vs*. the number of Froude can be given by visual evaluation of the images from the article and the simulations. According to the article, the

characteristics of the regimes presented in the experimental part (article) are reproduced in a similar way to those expressed by the simulation performed in this study in response to the speed range. The number of Froude, equation (23), is directly related to angular velocity and is linked to the type of drum operation regime, which can be classified using Table 2.

Table 2 - Number of Froude and operating regimes.

Angular velocity (rpm)	Froude number	Conclusion (scheme)
20	0,0539	Rolling
40	0,2155	Cascade
60	0,4849	Cataract
80	0,8621	Cataract to Centrifugal

Source: The author, 2022.

The speed of 20 rpm directs to a softer regime and more organized particle movement in the drum, but it is also notable for not expressing a good visualization of the mixing process, while there are still zones formed by particles of the same attributes after the simulation. The next regime, cascade, reveals the properties listed in the literature at the start of the test by composing a light format of "S" in the particle bed in the drum. Furthermore, there is more dynamic between particles. However, sphere homogeneity (mixture) has not been achieved; there are still considerable areas with particles with the same characteristics.

The speed of 60 rpm exhibits cataract regime characteristics since that demonstrates particle disassociation from the drum wall in region 1 with higher intensity and in an individualized way. At 80 rpm, greater dynamics between particles are presented; this state can be considered as a transition range between the cataract and centrifugal regimes. It's interesting how quickly a greater mixing process can be expressed in these regimes. However, it is significant to mention that cataract and centrifugation regimes are not the most widely used in industrial mixing processes (HENEIN *et al.,* 1983).

The internal angles of the packaging were used for velocities ranging from 20 to 80 rpm for $t \approx 6$ s to evaluate the study quantitatively. The simulated results showed a profile very similar to those shown in the article, as evidenced by the regime profiles in Figure 18 and

Figure 19, as well as the comparison of internal angles in Table 3 and Figure 20. To summarize, DEM simulations of granular materials using LIGGGHTS® software were able to reproduce well the results expressed in the article data.

Table 3 - Speeds vs. angles.

Speed (rpm)	Article	Simulation	Speed (rpm)	Article	Simulation
20	35°	36°	60	49°	50°
40	42°	42º	80	-	-

Source: The author, 2022.

Figure 18 - Real experiments of the article.

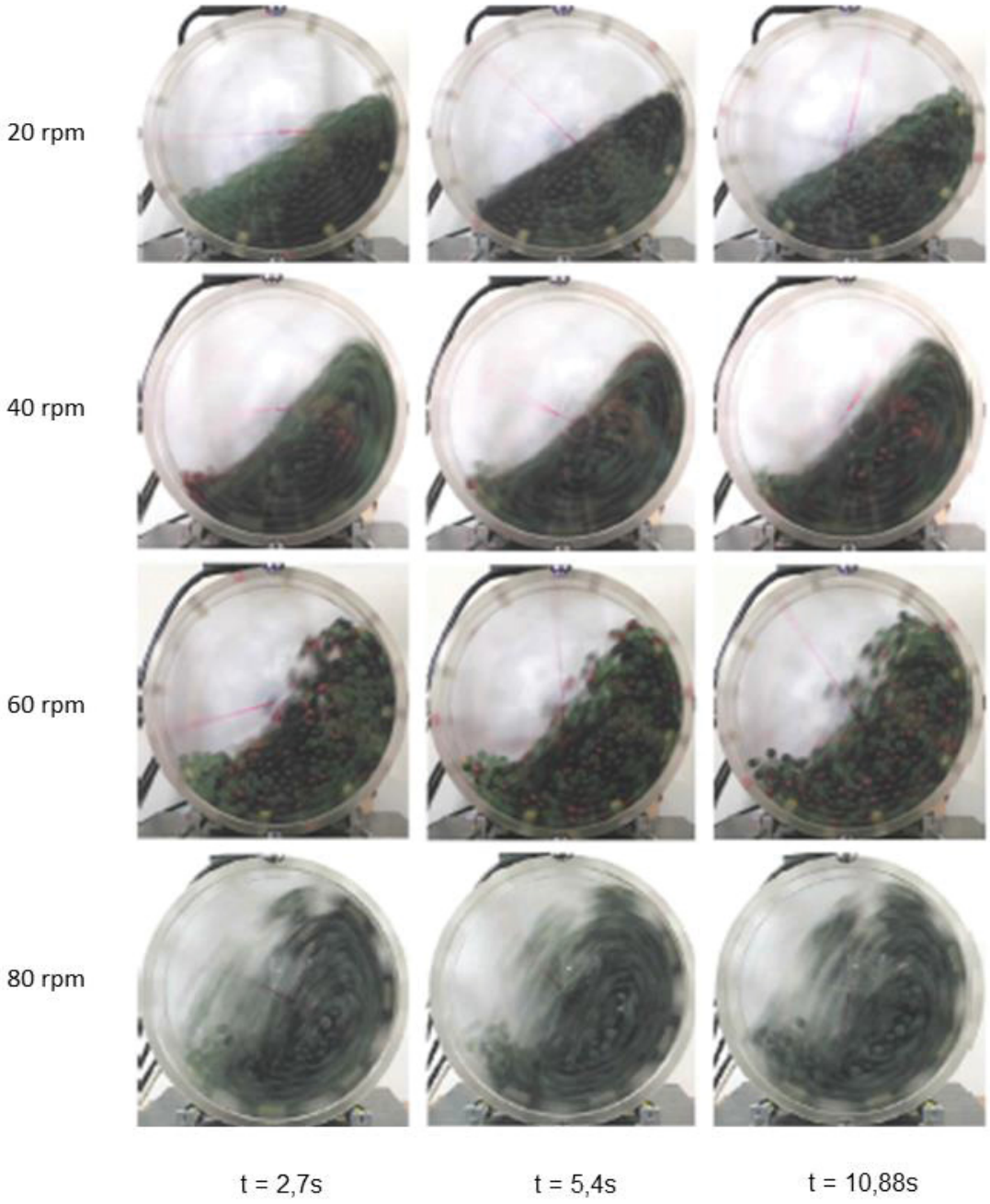

Source: Adapted from Xu *et.al.,* 2010.

Figure 19 - Simulation of the conditions applied in the article.

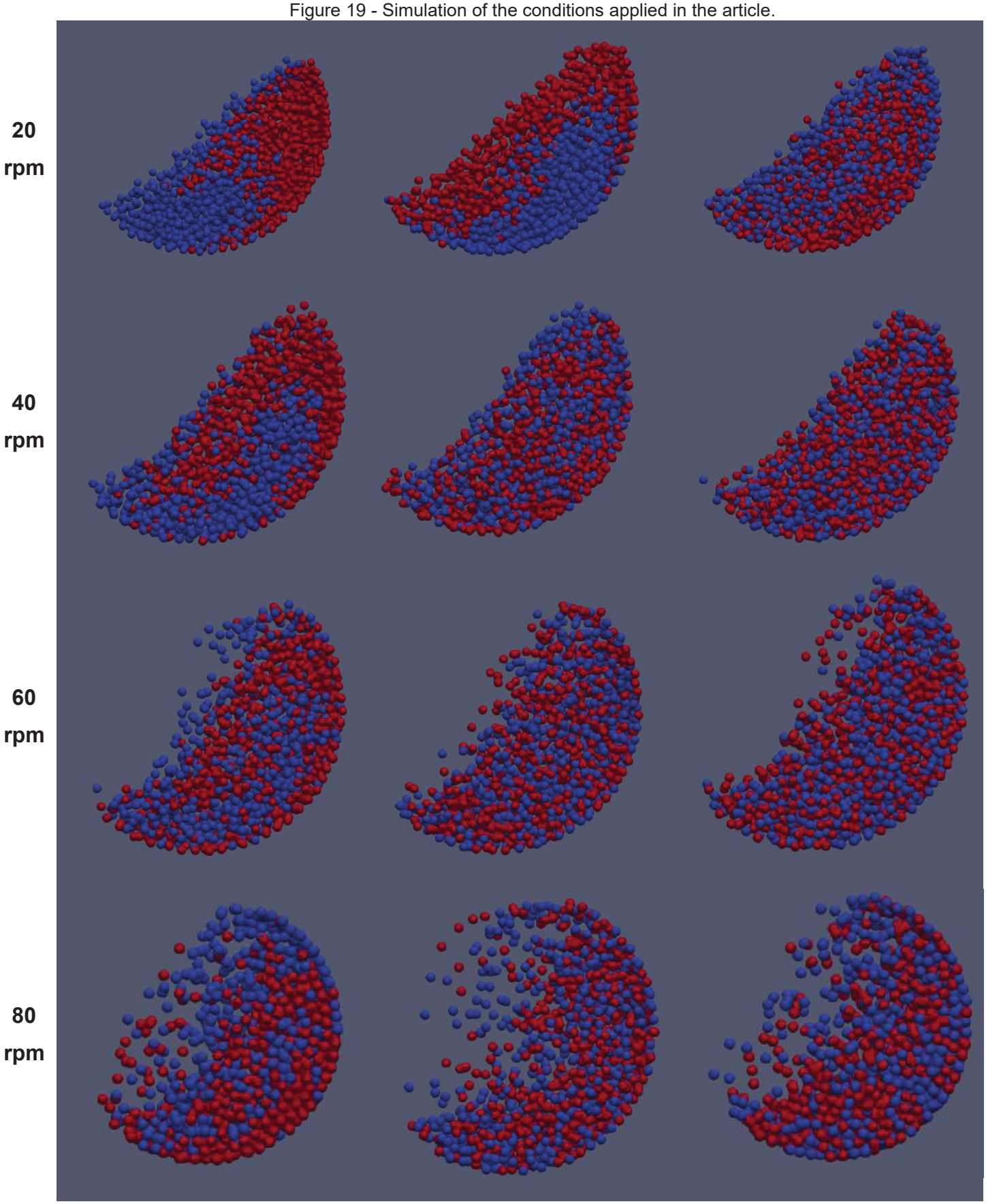

t ≈ 3 s **t ≈ 6 s** **t ≈ 10 s**

Source: The author, 2022.
Figure 20 - Angle views.

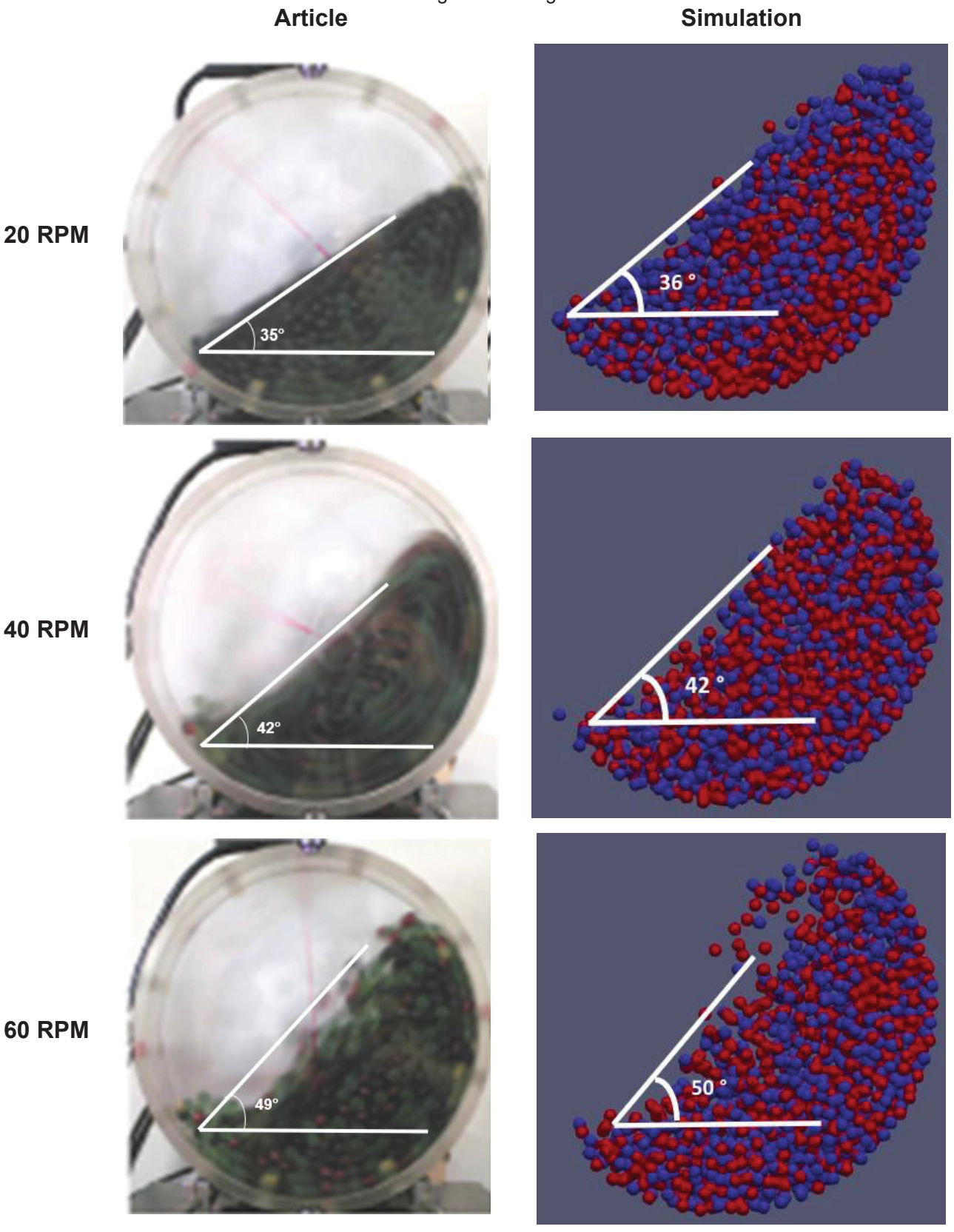

Source: The author, 2022.

4. METHODOLOGY

The components used in the practical experiments and their methods are described in this section; that is, the methodologies used to achieve the specific objectives addressed in Item 1.1. In general, it wants to use calibration parameters to investigate the friction coefficients (static and rolling) of granulated sugar. It was chosen as a research material mainly due to the rarity of information in the literature and the descriptive requirement that this parameter provides in the food sector for the mixing process, in addition to being one of the most often used items in Brazil.

4.1. PREPARATION OF SAMPLES

Guarani® crystal sugar was used for the sieving process. Eleven sieves were chosen to achieve a more homogeneous distribution of the particles. The sample was sifted, arranged from largest to smallest opening, and displayed the following programming characteristics, below. Then they were dried in a desiccator at 40 °C for 24 hours.

- Sieving time: 10 minutes.
- Frequency: 500 Hz.
- Vibration amplitude: 41.

4.2. DETERMINATION OF THE MESHES

To measure the friction coefficient at a deeper level, the experimental development employed the biggest size of particles accessible (850 μm). Furthermore, two additional sizes (212 μm and 600 μm) were utilized in the test to investigate how particle size might affect the regime of particles in a rotating drum.

4.3. EQUIPMENT USED

To perform the drum rotation, an AKIYAMA MOTORS engine was used, with the series number AK280/0.63PF05R330SC, with a maximum yield of 280 rpm and power of 1.8 W. The images used to evaluate the proposed systems were taken with a Canon® EOS 6D Mark II camera. The measurement of the rotation speed was made by the KY-003 board, which uses the hall effect (based on a differential of magnetic

and electric field potential), connecting it to an Arduino board, model Uno R3. All the equipment was provided by UFPR.

The drum was considered to have an internal diameter of 48 mm, with a 25 mm depth (longitudinal direction), manufactured with stainless steel and used for sealing the system to an acrylic plate.

4.4. THE ROTATING DRUM

A drum was filled with 12.5 mL of crystal sugar, representing approximately 30% of the volume. The tests were carried out for particle sizes of 850 μm, 600 μm, and 212 μm at five different velocity levels (10 rpm to 50 rpm), see Figure 21.

Figure 21 - Rotating drum

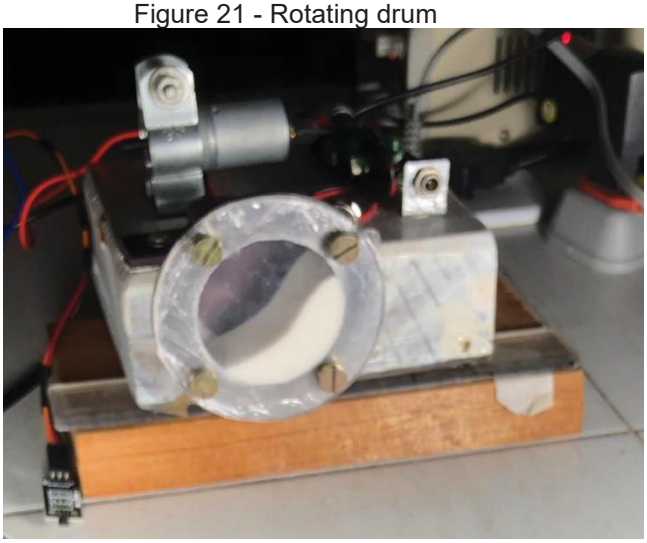

Source: The author, 2022.

4.5. SIMULATIONS

It presents the characteristics adopted and conditions for the simulation parameters in the present study.

4.5.1. Study delimitation

To search for a more specific point, one size of particle was chosen for a complete study of friction coefficients. A qualitative and quantitative search for the friction coefficient using 850 μm (size) and 10 to 50 rpm (speed) was conducted. For 600 μm, and 212 μm (10 rpm to 50 rpm), just a visual analysis to evaluate how the particle sizes and speeds can influence the drum regime.

The angle formed in the practical experiment was measured using Python, which allowed the image to be analyzed and describe the system's average angle.

4.5.2. Calibration of static and rolling friction coefficients

LIGGGHTS® software was used for static and rolling calibration, for 850 μm and 10 to 50 rpm. The main objective was to define the best value or range for the static and rolling coefficient that describes the behavior of granulated sugar in the test described in sections (4.4 and 4.5.1).

The analysis of the simulations was carried out by two factors (coefficient of rolling and static friction), analyzed in five levels, for 850 μm. In this way, the complete analysis presents $5^2 = 25$ simulations, see Table 4, for each speed (10 to 50 rpm). For the investigation of all possible combinations of friction coefficients, 125 simulations were run. The images produced as a result of this process made it possible to confirm the packing's angle of repose and compare them with actual observations.

Table 4 – Simulation planning.

Run	Rolling coefficient	Static coefficient	Run	Rolling coefficient	Static coefficient
Run 1	0	0	**Run 14**	0.5	0.75
Run 2	0	0.25	**Run 15**	0.5	1.0
Run 3	0	0.5	**Run 16**	0.75	0
Run 4	0	0.75	**Run 17**	0.75	0.25
Run 5	0	1.0	**Run 18**	0.75	0.5
Run 6	0.25	0	**Run 19**	0.75	0.75
Run 7	0.25	0.25	**Run 20**	0.75	1.0
Run 8	0.25	0.5	**Run 21**	1.0	0
Run 9	0.25	0.75	**Run 22**	1.0	0.25
Run 10	0.25	1.0	**Run 23**	1.0	0.5
Run 11	0.5	0	**Run 24**	1.0	0.75
Run 12	0.5	0.25	**Run 25**	1.0	1.0
Run 13	0.5	0.5	-	-	-

Source: The author, 2022.

4.5.3. Sugar

In general, commercialized sugar has sucrose ($C_{12}H_{24}O_{12}$) as its main component, which is a disaccharide formed by glucose and fructose molecules. It is regarded as one of the purest substances available in the industry, containing 99.9%

sucrose (CASTRO, 2013). Its low moisture content and lack of chemical additives, sugar is largely used in the food industry (MACHADO, 2012).

The sugar manufacturing process is fundamentally based on the extraction of and the concentration of sugarcane juice; it can be obtained as brown sugar, crystal sugar, refined sugar, and others (MACHADO, 2012).

Brazil is one of the world's largest sugar producers, accounting for 23 percent of global output. The Brazilian international market exported 771.73 thousand tons of sugar until June 2022, particularly in comparison to the 3.26 million tons exported in 2021 (ÚNICA, 2022).

4.5.4. Definition of simulation parameters

Sugar density has similar values regardless of type (refined or crystal), which is due to sucrose's crystalline morphological structure (SANTOS, L. *et. al.,* 2017). According to the IFA (Institute of Occupational Safety and Health of the German Social Accident Insurance), the average density of sugar is 1.5737 g/cm³ and according to studies by Santos, L *et.al.* (2017) for crystal sugar is 1.5763 g/cm³.

Ye *et. al.* (2019) used a predictive model to calibrate the Young modulus, comparing it to DEM results to determine which parameters are fixed and which will be variable, and it was discovered that it has little variability until a specified point. It was specified in the work of Chen, H. *et. al.,* (2017) that the maximum value of the module could be assumed to be 1000 times smaller than the real one. Sato *et. al.,* (2011) reported that the Young Modulus of sugar is 4.5 GPa.

The restitution coefficient, for example, has a low variability of value from a certain point and thus has little influence on the particle regime in the rotating drum. The value is set at 0.3 in the study by Ye *et. al.,* (2019), and the same value in the study by Singh *et. al.*, (2016). However, when working with sugar, this value is defined as 0.16 (SATO, *et. al.,* 2011). For Ramrez *et. al.,* 2010 studies, the average Poisson coefficient of crystal sugar was 0.21, while Singh *et. al.,* 2016 found it to be 0.252.

The rolling friction coefficient is extremely difficult to calculate. It is typically assumed to be very small or even ignored, as it was in the study by Chen, H. *et. al.,* (2017). Nevertheless, in DEM simulations, non-spherical particles are assumed to be spherical, and rolling friction coefficient values must be considered (KATTERFELD and

RÖSSLER, 2019). In view of this fact, it was considered that the contact model of the particles presents a rolling history, considering the Hertz model.

The rotating drum's wall was supposed to have the same properties as the particles. In addition, no non-contact forces were included during the simulations.

The Rayleigh waves were calculated using equation (21) and their timestep was assumed to be $1x10^{-6}$. Due to the computational effort, all simulations were performed with spherical particles, and the total time was set for a simulation time of 2 seconds. Table 5 presents the values to be assumed for this study based on data from the literature and experimental data. The code for simulation is presented in APPENDIX 2 – Script for granulated sugar.

In general, the literature presents the calibration of one or two parameters while leaving the others unchanged. The static and rolling friction coefficients are generally applied (HE *et. al.,* 2019; YE *et. al.,* 2019).

Table 5 - Parameters defined.

Parameter	**Value**
Density (kg/m³)	1570
Young Module (Pa)	4.5×10^{8}
Poisson coefficient	0.23
Restitution Coefficient	0.16
Timestep (s)	1×10^{-6}
Simulation time (s)	2
Gran model	hertz tangential history rolling friction epsd2

Source: The author, 2022.

5. RESULTS

The LIGGGHTS® is used to characterize granular materials, notably, those utilized in industrial applications (CFDEM, 2011 and 2016), see more information in Section 2.8. The observations and results of the LIGGGHTS® simulation are presented here.

5.1. FIRST OBSERVATION

The first observation is that the change in particle speed influences the regime present in the rotating drum, as seen in the images, in Figure 22, which range from a rolling system to a cascading system. The gentler the variability, the larger the particle size. When increasing the rotational speed, the regimes slightly change. For example, at 10 rpm, the current regime is rolling. When 50 rpm is present, for the larger particle, the cascade regime becomes less visible but still present, making this regime more visible for the smallest particle.

Figure 22 - Speed vs. mesh.

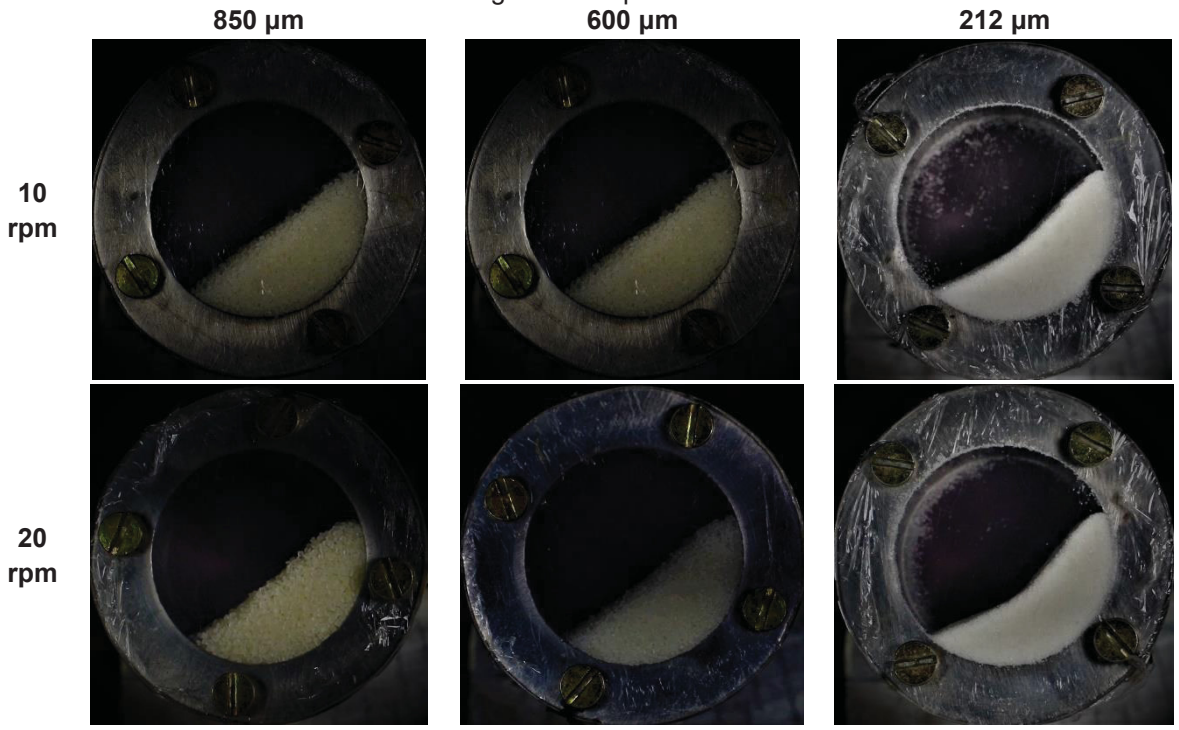

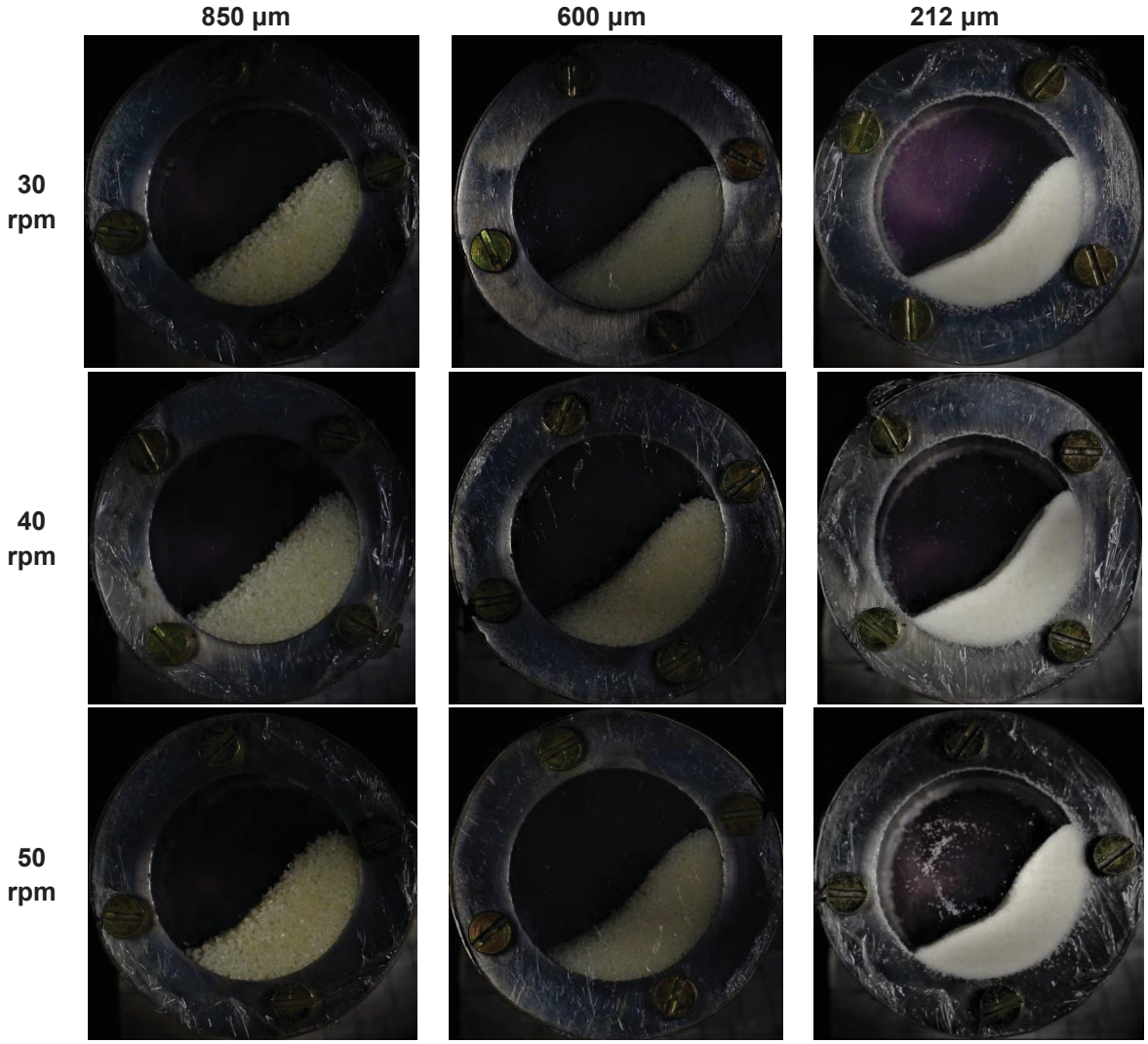

Source: The author, 2022.

The angle of repose of the particles in the revolving drum changes as the rotational speed goes from 10 to 50 rpm, as shown in Figure 23. The angle ranges ± 5 degrees between the lowest and greatest speed values for particles of 850 µm and 600 µm. However, for 212 µm, at greater speeds, two angles arise owing to the more obvious cascading regime.

Figure 23 - Speed vs. mesh 850, 600, and 212 µm.

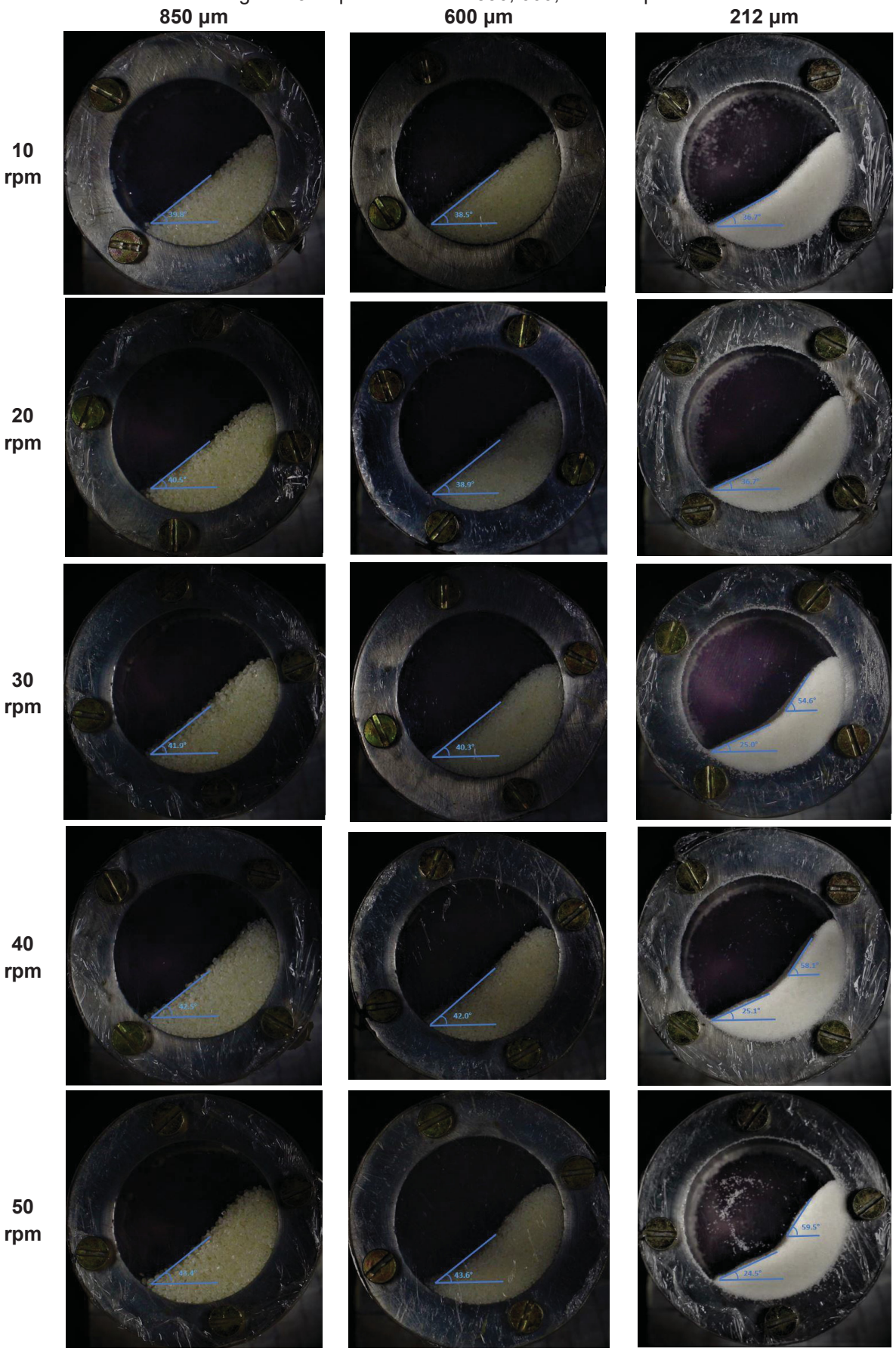

Source: The author, 2022.

5.2. FURTHER INVESTIGATION ON 850 μm

Further investigation of the particle size of 850 μm reveals that the modification of friction coefficients has a direct effect on particle interaction as well as particle velocities within the drum.

One of the most important findings is that the coefficient of static friction is critical in defining granular flows because, without it, the particles remain static in the drum. That is, even though the drum is moving, the particles barely move. They remain, as if in feathery swings, but without establishing a regime, see Figure 24. When the rolling coefficient gradually increases, and the static coefficient remains zero, there is not a slight effect on particle velocity.

Figure 24 – Static Friction coefficients = 0.0.

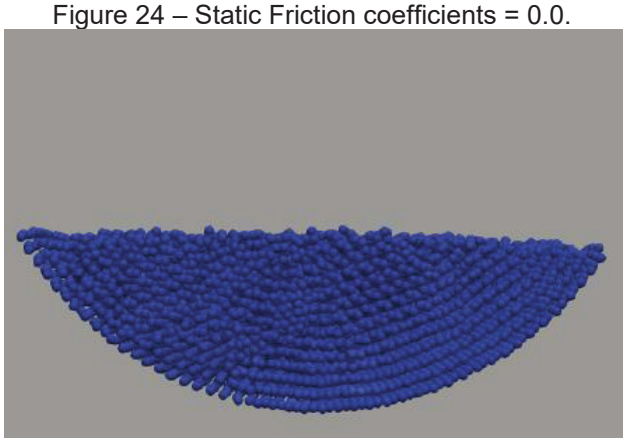

Source: The author, 2022.

The coefficient of rolling friction is frequently overlooked, as mentioned in the literature. However, this is not the case for non-spherical particles, as in this study. When these parameters are gradually raised, the particle angular values change, slightly increasing.

The active layer of particles becomes more visible as the coefficients of static and rolling friction rise. Especially when the static is between 0.5 and 0.75, it's possible to see greater velocity at the particle. This was already predicted since the particles have a higher resistance to mobility. The velocity profiles are possibly to be seen in Figure 25 to Figure 29.

As the particles are identified with the speed factor in the images, bluer indicates low speed, and as they become redder, the speed rises.

Figure 25 – Rolling Friction coefficients = 0.0.

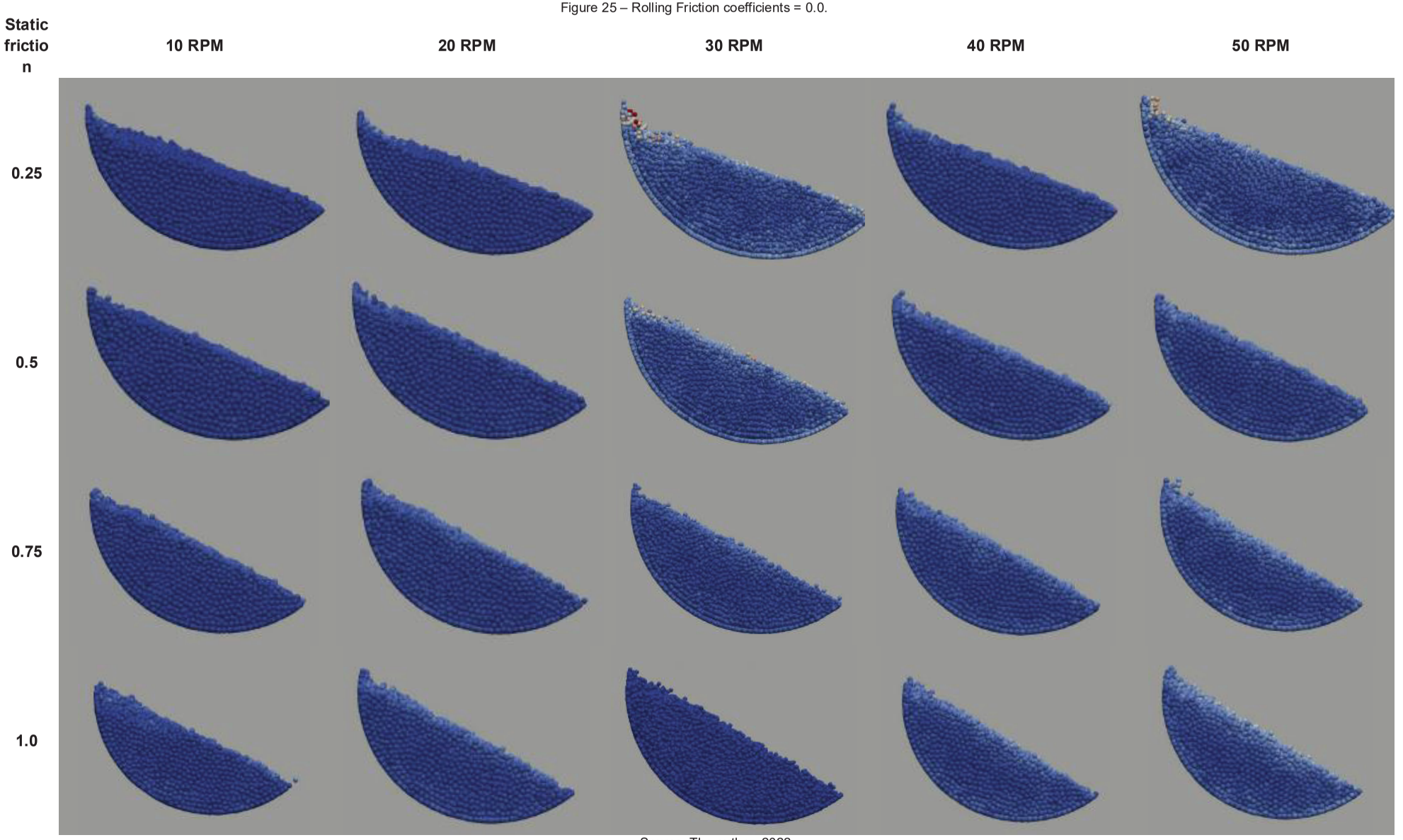

Source: The author, 2022.

Figure 26 – Rolling Friction coefficients = 0.25.

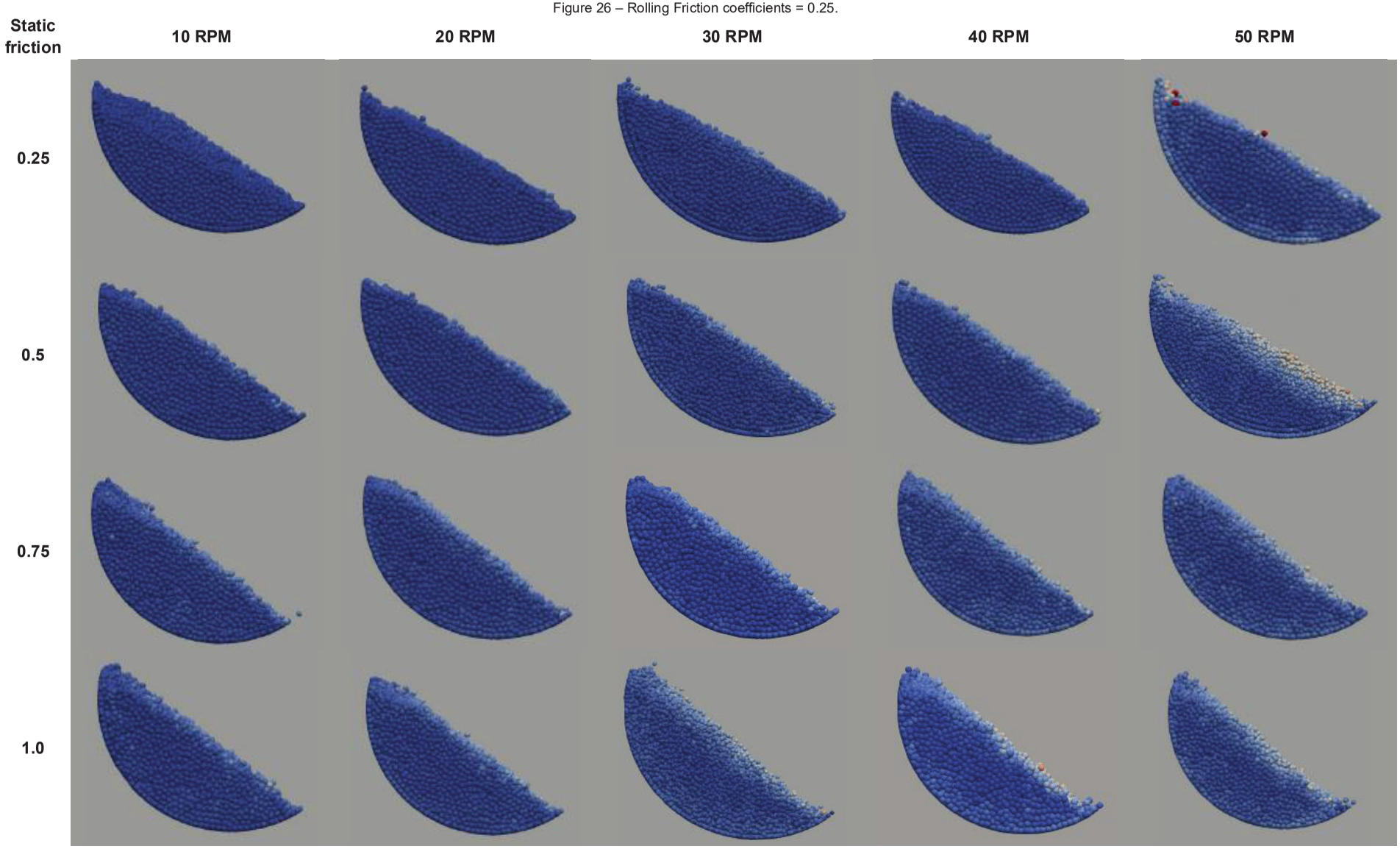

Source: The author, 2022.

Figure 27 – Rolling Friction coefficients = 0.5.

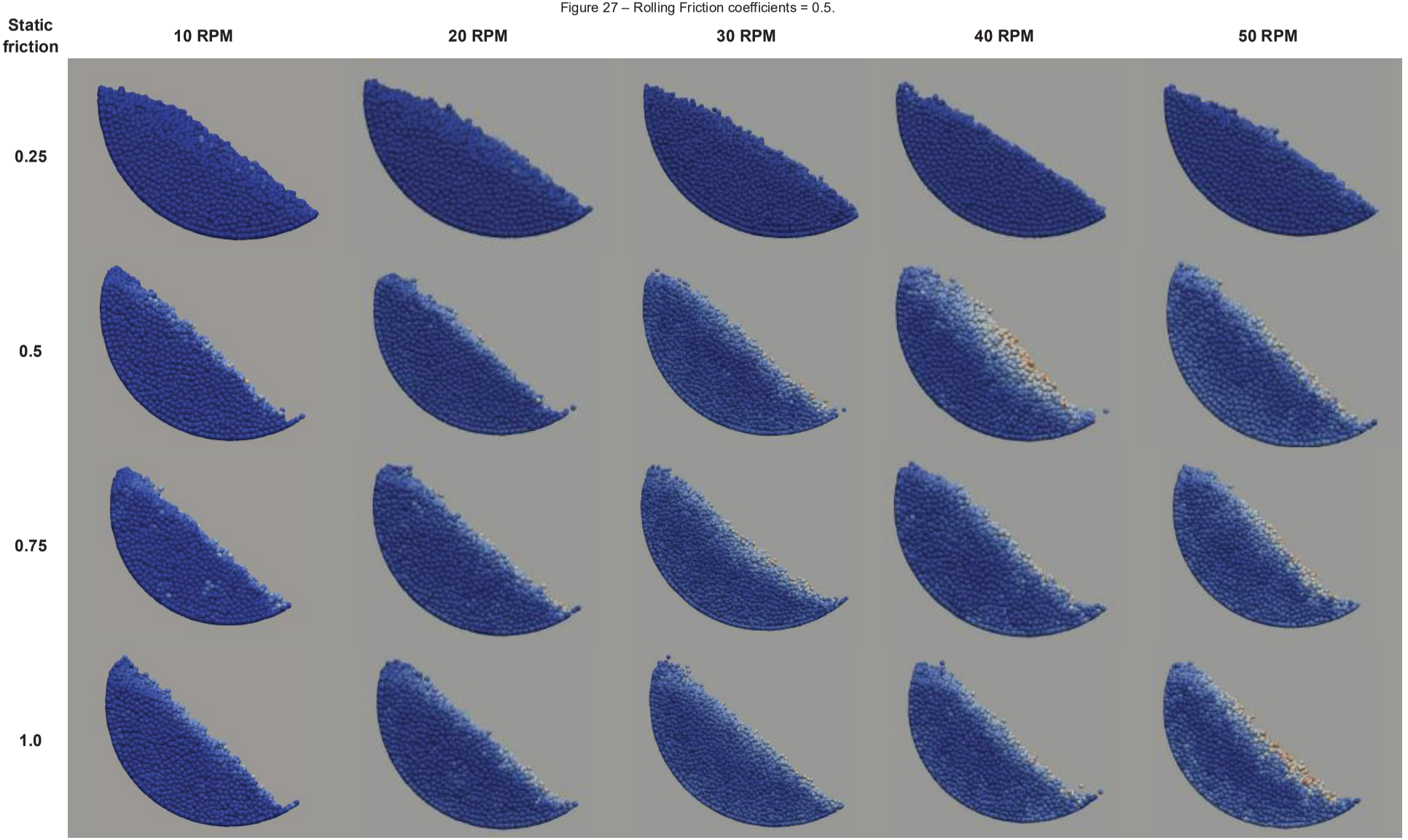

Source: The author, 2022.

Figure 28 – Rolling Friction coefficients = 0.75.

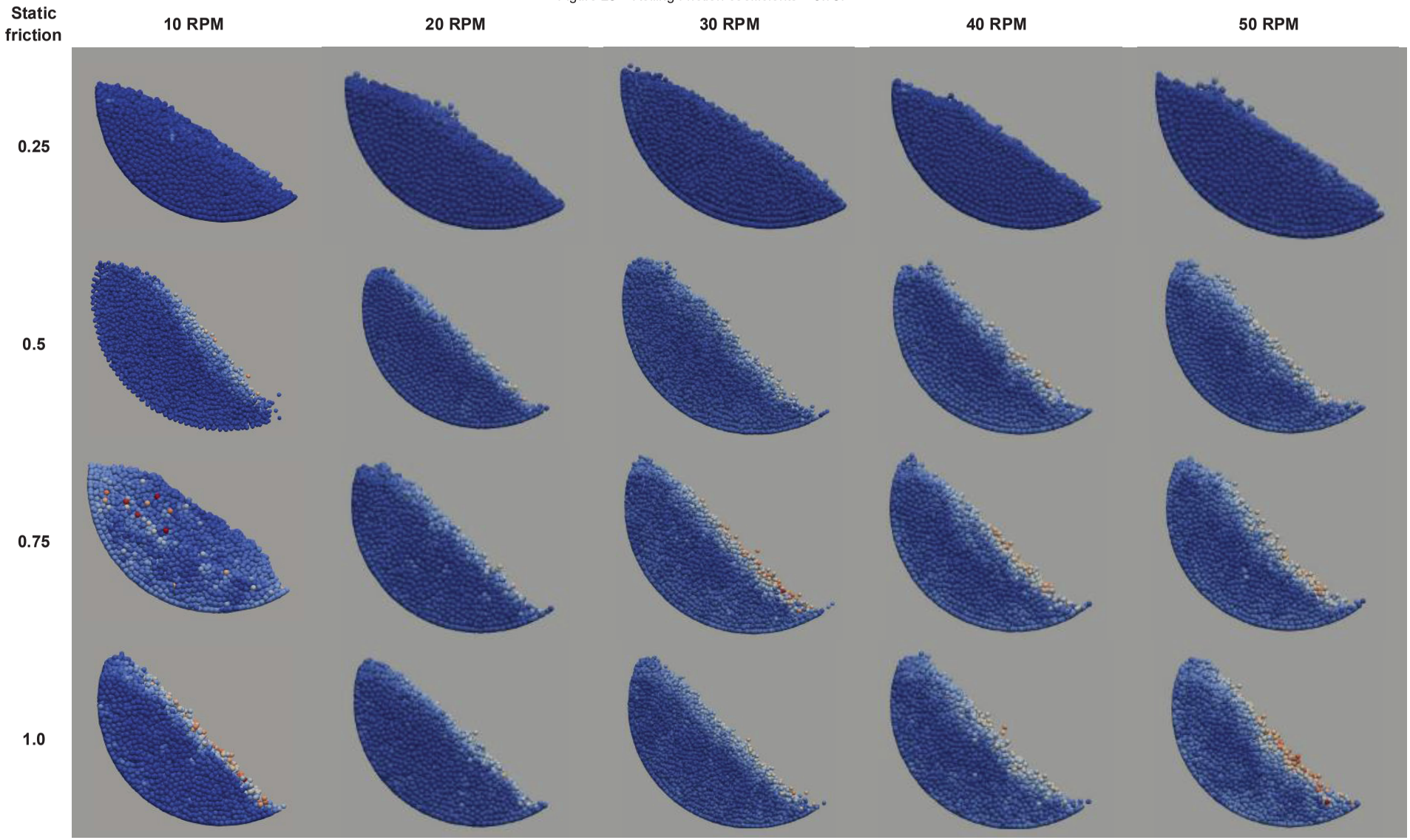

Source: The author, 2022.

Figure 29 – Rolling Friction coefficients = 1.0.

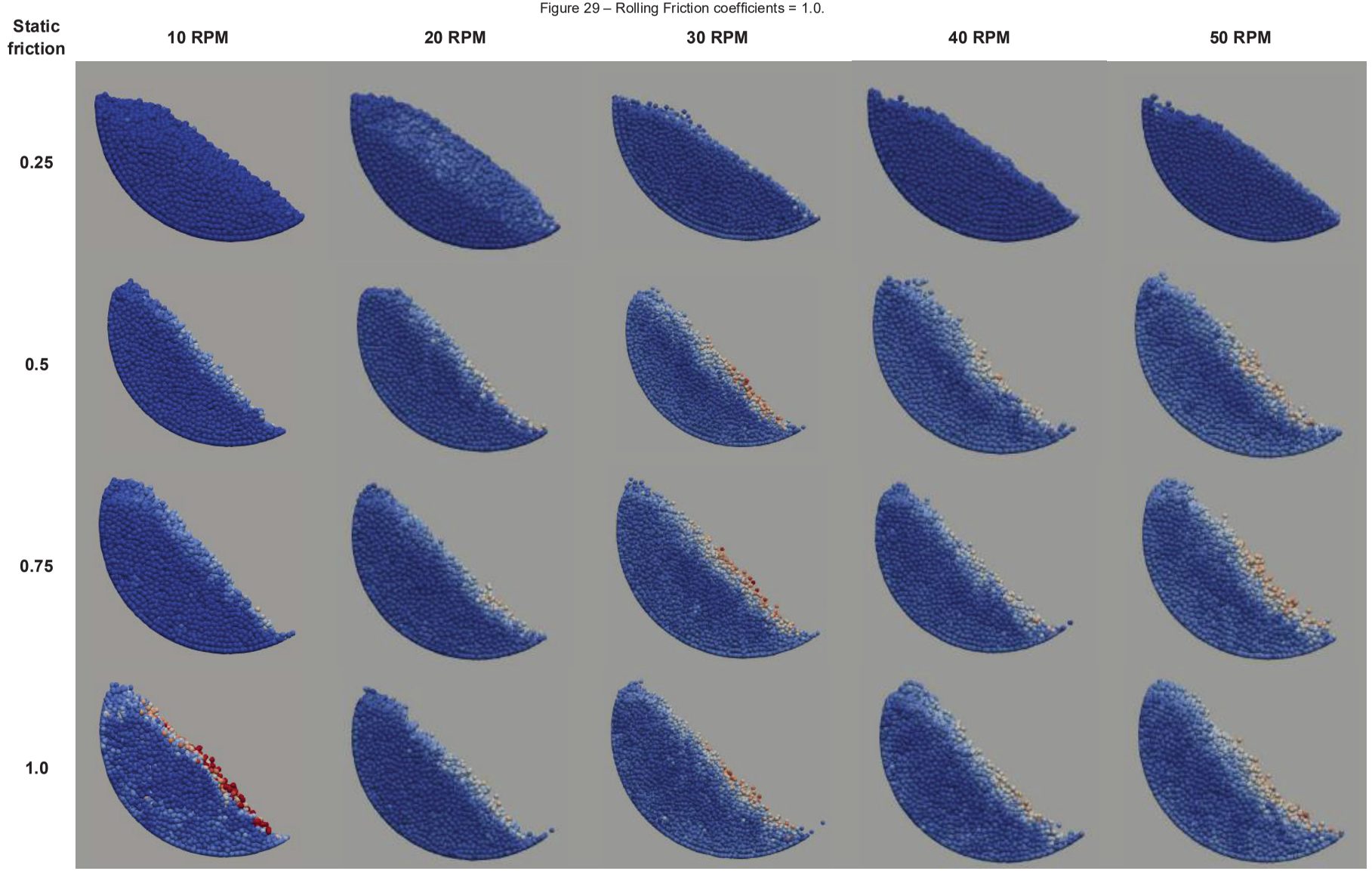

Source: The author, 2022.

Table 6 shows the Froude numbers, equation (23), which is directly connected to angular velocity, for each speed in this investigation. All the speeds present in the rolling regime are observed in Figure 22 for 850 µm.

Table 6 - Number of Froude for 850 µm.

Angular velocity (rpm)	Froude number	Angular velocity (rpm)	Froude number
10	5.89×10^{-5}	**40**	9.43×10^{-4}
20	2.36×10^{-4}	**50**	1.47×10^{-3}
30	5.31×10^{-4}	-	-

Source: The author, 2022.

With the simulations, using the LIGGGHTS® program, it is possible to measure the angles created in the particle packing. These will then be used to identify which set of friction coefficients best characterizes the sugar grain regime in the rotating drum. Figure 30 to Figure 34 show the comparison of the simulated angle (green points) and the real angle (blue points).

Figure 30 – Comparison between simulated (green) and real (blue) angles for 10 rpm.

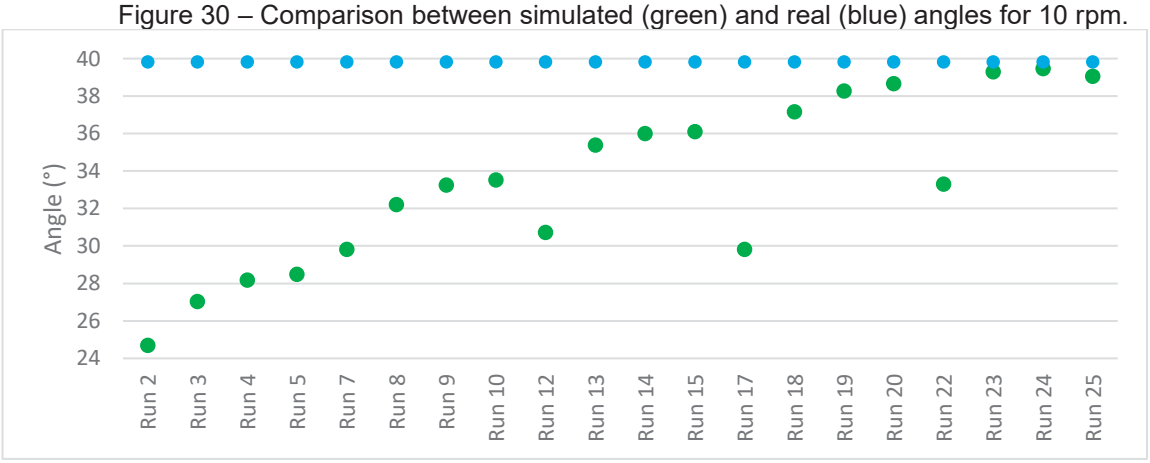

Source: The author, 2022.

Figure 31 – Comparison between simulated (green) and real (blue) angles for 20 rpm.

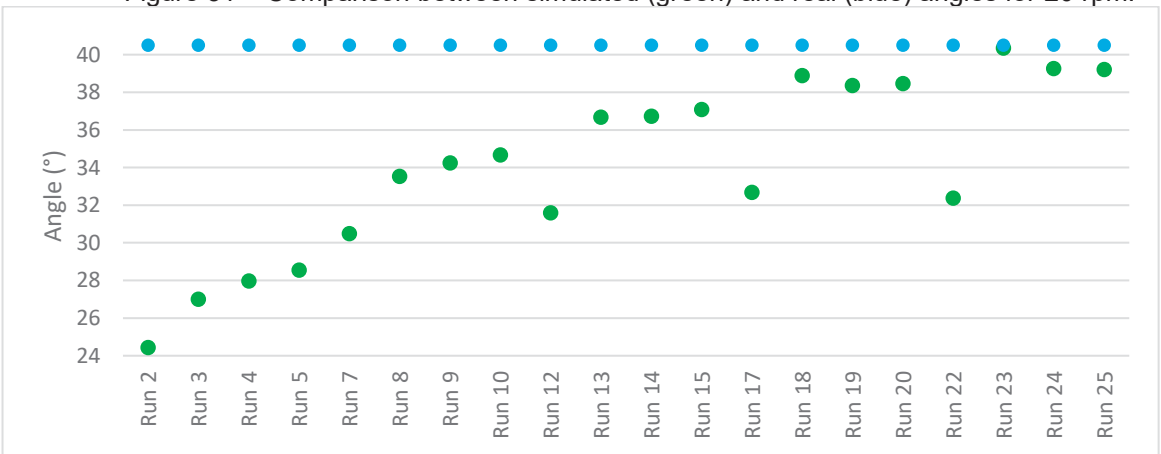

Source: The author, 2022.

Figure 32 – Comparison between simulated (green) and real (blue) angles for 30 rpm.

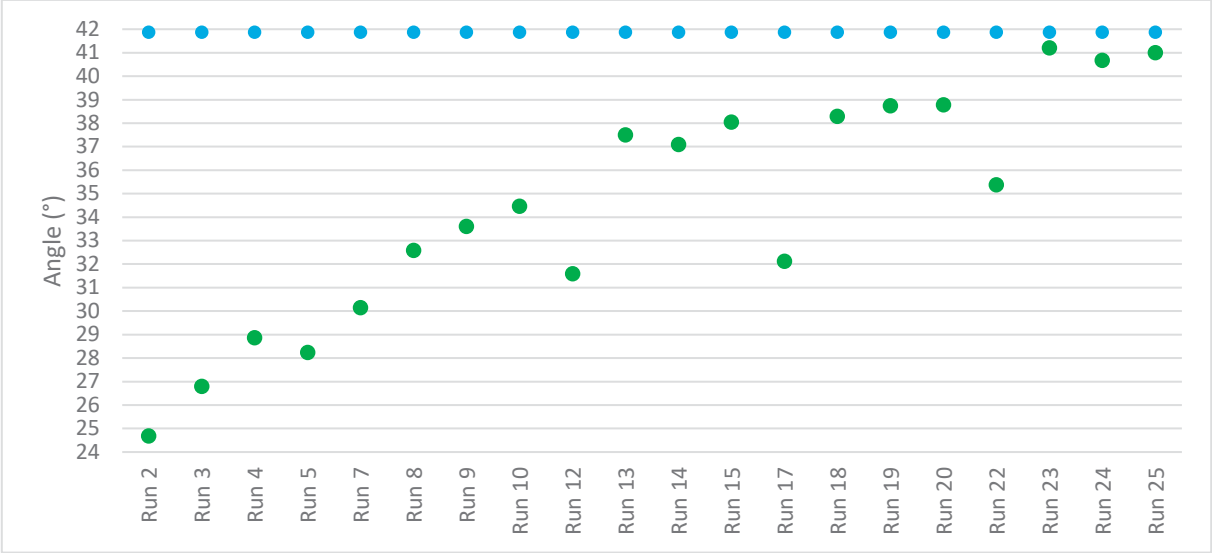

Source: The author, 2022.

Figure 33 – Comparison between simulated (green) and real (blue) angles for 40 rpm.

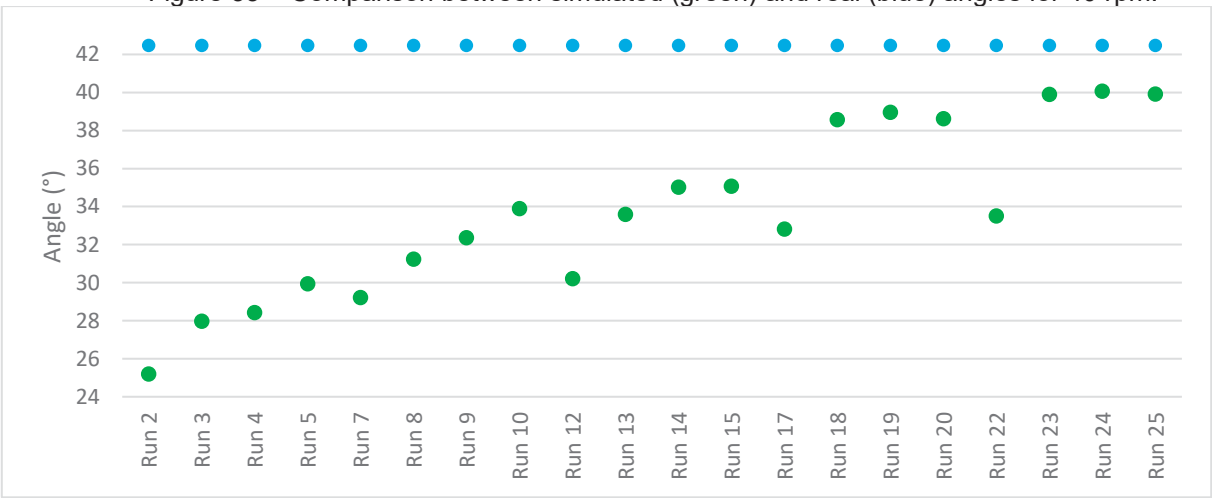

Source: The author, 2022.

Figure 34 – Comparison between simulated (green) and real (blue) angles for 50 rpm.

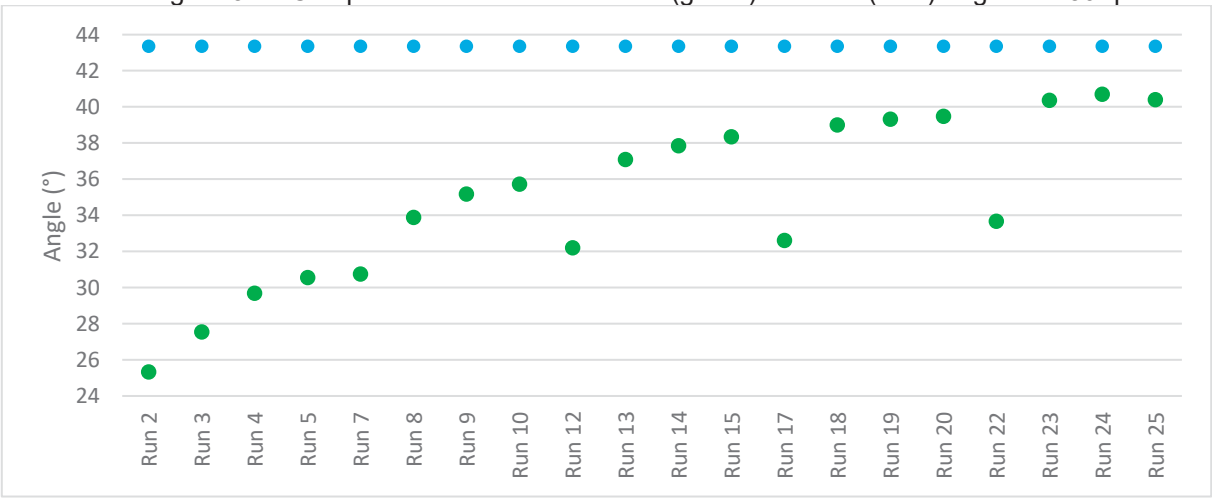

Source: The author, 2022.

Some weighting can be indicated in the image. When the coefficient of rolling friction is under 0.75, they may be dismissed as possible coefficients, and when the coefficient of static friction is equal to or less than 0.25, they do not represent the system since the angle created is considerably lower than the true one. In this context, the sugar's rolling friction coefficient should be between 0.75 and 1, while the static friction coefficient greater than or equal to 0.5.

Figure 35 to Figure 39 illustrates how static and rolling friction coefficients affect the angle generated by particles inside the rotating drum. The modification of the coefficients has a direct influence on the angles. The first point to consider is that the static friction coefficient is the most important influencer, but the rolling coefficient also has an effect on the packing and cannot be neglected in the simulations.

Figure 35 – Friction coefficients effects 10 rpm.

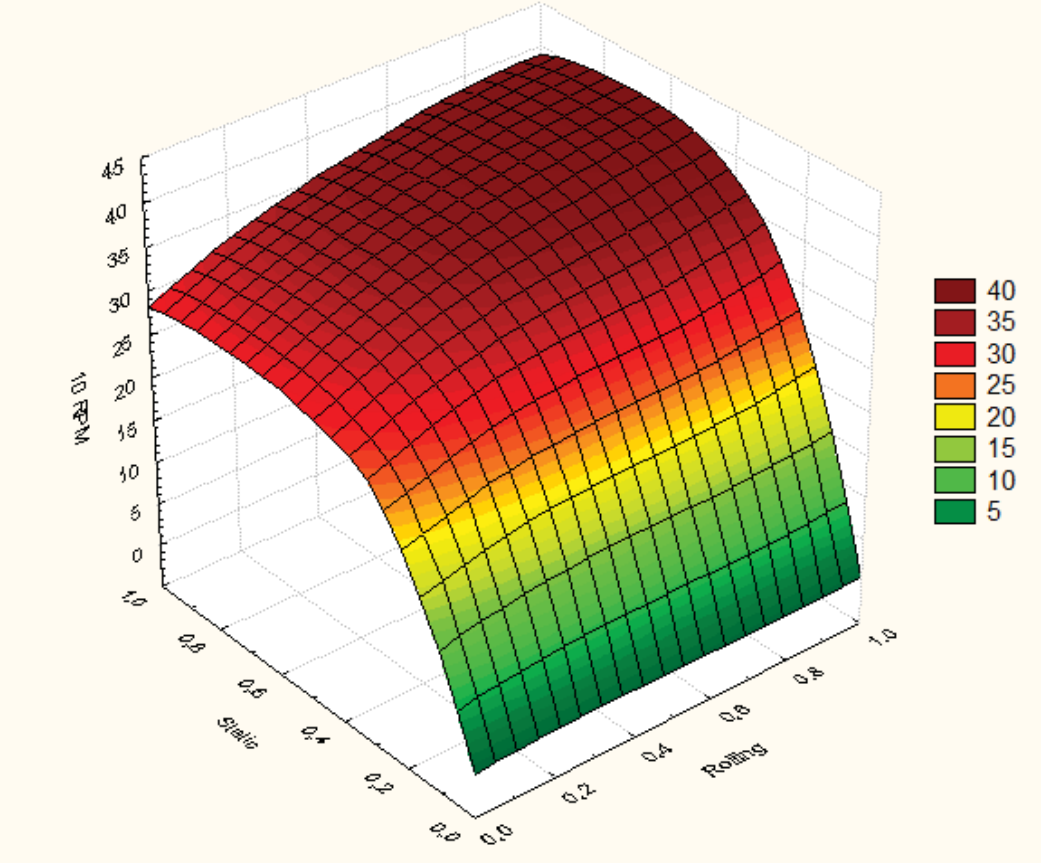

Source: The author, 2022.

Figure 36 – Friction coefficients effects 20 rpm.

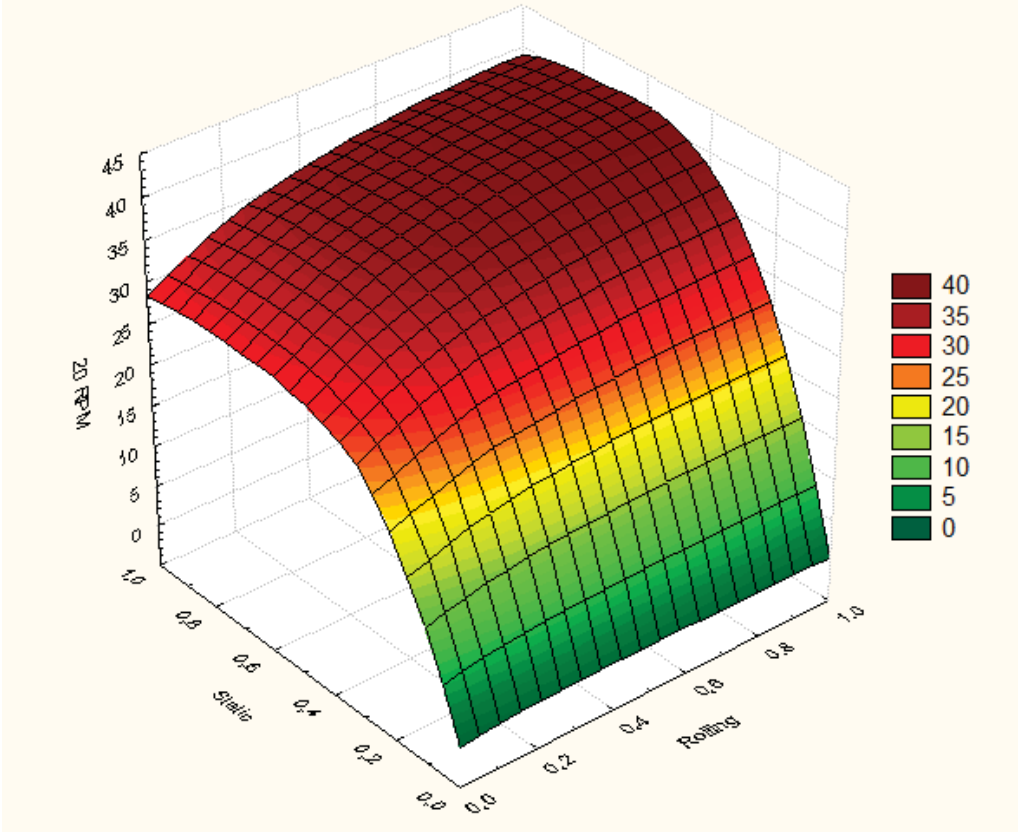

Source: The author, 2022.

Figure 37 – Friction coefficients effects 30 rpm.

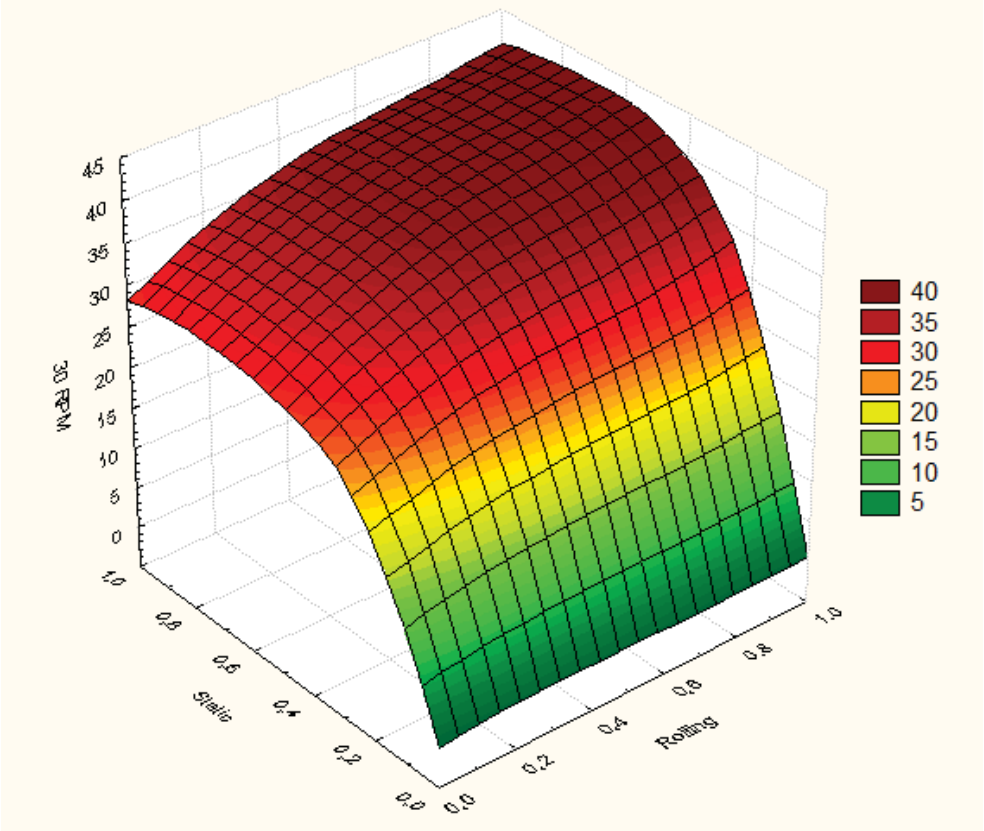

Source: The author, 2022.

Figure 38 – Friction coefficients effects 40 rpm.

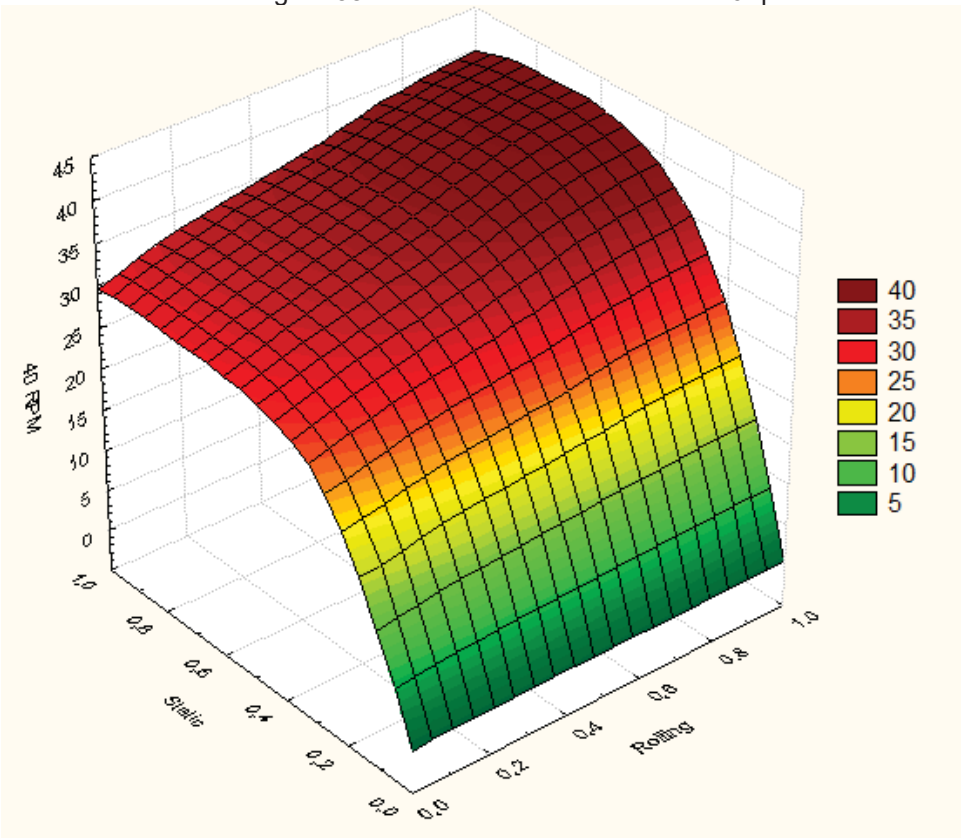

Source: The author, 2022.

Figure 39 – Friction coefficients effects 50 rpm.

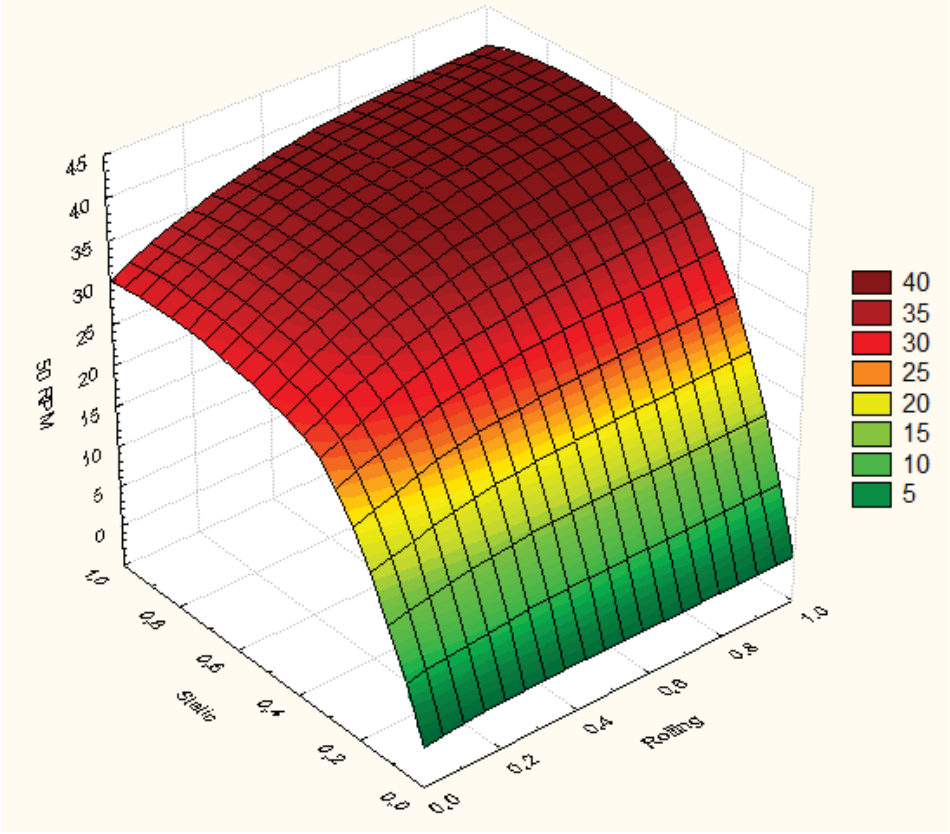

Source: The author, 2022.

Both coefficients have statistically significant effects on the formation of the angle; as shown in the graphs, the coefficient of static friction less than 0.25 does not show significant variations in the samples, but the other parameters and variations (rolling from 0 to 1 and static from 0.5 to 1) do. When compared to the data set, the coefficient of static friction is the key component with the greatest relevance in the results.

A quantitative comparison, angle verification, and a qualitative visual evaluation of the behavior of the particles in the drum must be accomplished to choose the optimum dataset.

Among the 125 simulated scenarios, the ones with the closest values to the experimentally obtained angle were listed in Table 7. It shows the comparison of actual and simulated values, as well as the set of friction coefficients responsible for the output. Figure 40 shows a visual comparison of each case with the best performance.

Table 7 - The connection between the results and the effective angle

Velocity (rpm)	Real Angle	Run	Rolling Coefficient	Static Coefficient	Simulated Angle
10	39.83º	24	1	0.75	39.47º
20	40.50º	23	1	0.5	40.34º
30	41.87º	23	1	0.5	41.20º
40	42.46º	24	1	0.75	40.06º
50	43.36º	24	1	0.75	40.70º

Source: The author, 2022.

There is a lower fluctuation between the true value of the angle generated by the particles within the rotating drum and those obtained by simulation. The profile presented in the experimental testing appears to indicate smooth rolling; that is, the particles roll from one end of the drum to the other without causing big waves on the surface.

According to these observations, the potential range of granulated sugar friction coefficients is near to or equal to 1 for rolling and between 0.5 and 0.75 for static.

Figure 40 – Comparison of the experimental and simulation parts.

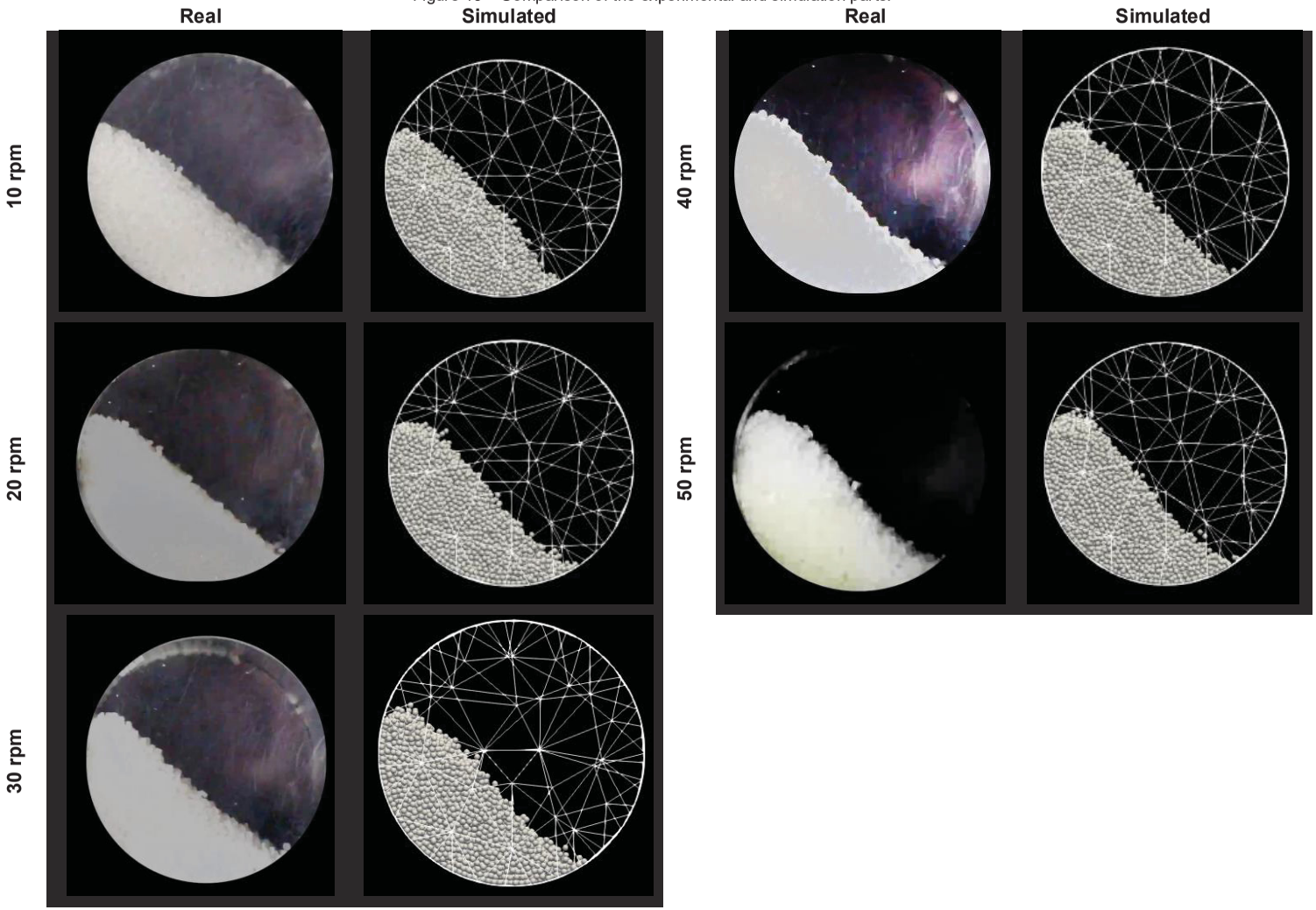

Source: The author, 2022.

6. CONCLUSION

Despite being a relatively recent field of research in the scientific community, the discrete element approach has undergone rapid development, from its theoretical foundations to the auxiliary analysis software that is pretty good at forecasting flows of granular materials. This method effectively predicts the behavior of granular flows by using a mathematical approach (Langregian), considering all levels of contact categories and how they function.

There are two very important boundary requirements for the contact mechanism, in particular (rigid and deformable spheres). Furthermore, several models can be used to represent them. However, it is critical to evaluate each instance separately based on the foundational fundamental concepts it is built on, rather than just its numerical simplicity. Considering the data found in the literature, DEM exhibits a strong capacity to forecast the behavior of granular materials and offers findings that are consistent with those obtained via experimentation.

From a wider perspective of this study, it is possible to see the impact that granulometry and rotational speed might have on the grain operating regime inside the rotating drum. More intense regimes are seen in the cascade as the particle diameter reduces and the velocity rises.

Simulations, such as LIGGGHTS®, are a tool with endless possibilities to characterize granular flows. For a more micro perspective, which is conducted in this work, the definition of the rolling and static friction coefficients of granulated sugar for a specific granulometry and speed (850 μm and 10 to 50 rpm). However, determining the boundary conditions is crucial information for precisely defining the pair of coefficients.

Evaluation of the potential for friction coefficients was made possible by the successful completion of the experimental planning (5^2) for 850 μm and each speed (10 to 50 rpm). Some of these points were wildly unrealistic (static friction coefficient equal to zero). These results were compared with the models as the experimental procedures were carried out and the angles of repose were established. Thus, it was determined that for this situation, close to 1 for the rolling friction coefficient and between 0.5 and 0.75 for the static one would be the most descriptive combination.

As demonstrated, the use of Benchmark models can produce good outcomes in simulations. However, the simulation by itself is insufficiently compelling; based on

real testing with the rotating drum, the optimal range of friction coefficients for granulated sugar may be described.

The results of this investigation provide insight into how the coefficients of friction for sugar grains behave. However, further research is required to completely explain them. As a result, the parameters utilized can be adjusted, though it has substantial implications for the study of granular materials by LIGGGHT® employing the discrete element approach.

REFERENCE

ABI-MANSOUR, A. PyGran: An object-oriented library for DEM simulation and analysis. **Softwares**. v.9 p. 168-174, 2019.

ANGUS, A. *et al.* Calibrating friction coefficients in discrete element method simulations with shear-cell experiments. **Powder Technology.** v. 372, p. 290–304, 2020.

ASMAR, B. N. *et. al.* Validation tests on a distinct element model of vibrating cohesive particle systems. **Computers and Chemical Engineering**. v. 26, p. 785–802, 2002.

AYENI, O. O. *et. al.* A discrete element method study of granular segregation in non-circular rotating drums. **Powder Technology.** v. 283, p. 549–560, 2015.

BERTHIER, Y. SECTION 8.2 - Background on Friction and Wear. *In:* LEMAITRE, J. Handbook of Materials Behavior Models, Academic Press, 2001, p. 676-699. Available in < https://www.sciencedirect.com/science/article/pii/B9780124433410500740 >. Access: 01 May. 2022.

BOATENG, A. A. Rotary Kilns: Transport Phenomena and Transport Processes. In: BOATENG, A. A. **Basic Description of Rotary Kiln Operation**. 2 ed. Elsevier, 2016, p 13-26.

BRANDÃO, R. J. **Estudo da segregação de material granular em tambor rotatório empregando a abordagem numérica lagrangeana.** 2017. Dissertation (Master's degree in Chemical Engineering) - Federal University of Uberlândia, Minas Gerais.

CAMPOS, L. F. O. **Desenvolvimento de metodologia para o uso de partículas viscoelásticas no método dos elementos discretos**. 2016. Dissertation (PhD in Chemical Engineering) - Federal University of Rio de Janeiro. Rio de Janeiro

CARLI, E. M. *et. al.* APLICAÇÃO DO MÉTODO DOS ELEMENTOS DISCRETOS EM UM TALUDE: COMPARAÇÃO ENTRE A SIMULAÇÃO COMPUTACIONAL E A

PRÁTICA. **Salão do conhecimento Unijuí: ciência para a redução de desigualdades**. 2018.

CASTRO, H. F. **Processos Químicos Industriais II: Apostila 1 - INDÚSTRIA AÇUCAREIRA**. University of São Paulo, Lorena School of Engineering, 2013.

CFDEM. Docs. Available in:< https://www.cfdem.com/media/DEM/docu/Section_intro.html>. Access: 22 Ago 2022;.

CFDEM® Project. LIGGGHTS OPEN SOURCE DISCRETE ELEMENT METHOD PARTICLE SIMULATION CODE. Available in: < https://www.cfdem.com/liggghts-open-source-discrete-element-method-particle-simulation-code>. Access: 22 Ago 2022.

CHEN, H. *et. al.* Effect of Young's modulus on DEM results regarding transverse mixing of particles within a rotating drum. **Powder Technology**. v. 318, p.507-517, 2017.

CUNDALL, P. A.; HART, R. D. Numerical Modeling of Discontinua. **International Journal for Computer-Aided Engineering and Software**, Minneapolis, MN, USA, p. 231-243, 1992.

DAVIDSON, J. F. *et. al.* Granular Motion in a Rotary Kiln: The transition from avalanching to rolling. 2000. **Powder and Particle**. n. 18, p. 149-156.

ENDRES, S. C. et al. A review of contact force models between nanoparticles in agglomerates, aggregates, and films. **Journal of Aerosol Science.** v. 153, 2021.

FAZEKAS, S. **Distinct Element Simulations of Granular Materials.** 2007. Ph.D. thesis (Ph.D. in Physics) - Department of Theoretical Physics University of Technology and Economics of Budapest. Hungary.

GARCIA, G. C. R. **Estudo do comportamento ao dano por choque térmico de um concreto refratário, contendo agregados de andaluzita, sinterizado em diferentes temperaturas.** 2010. Dissertation (Master's degree in Metallic, Ceramic and Polymeric Materials) - Lorena School of Engineering, University of São Paulo, Lorena, 2010.

GOMES, A. V. S. **Estudo do Acoplamento do Método dos Elementos Finitos e dos Métodos dos Elementos Discretos na Análise de Interação Solo-Estrutura**. 2014. Dissertation (Master's degree in Mechanical Engineering) - State University of Campinas. Campinas.

HABIB, M. *et. al.* Discrete Element Modeling (DEM) of the Vertically Vibrated Particle Bed. **Particulate Science and Technology: An International Journal**, p. 257-273, 2014.

HALLIDAY, D. **Fundamentals of physics:** Mechanics. 10th. ed. Rio de Janeiro: LTC, v. 1, 2018.

HE, P. *et. al.* Parameters by the Back-Propagation Neural Network Based on the Genetic Algorithm: Recycled Polyurethane Powder. **Materials**. 2019.

HEILBUTH, R. R. **Estudo da mistura e segregação de material granular em tambor rotatório com suspensores empregando a abordagem numérica Lagrangeana.** 2017. Dissertation (Master's degree in Chemical Engineering) - Federal University of Uberlândia, Uberlândia.

HENEIN, H. *et. al.* Experimental Study of Transverse Bed Motion in Rotary Kilns. **Metallurgical and Materials Transactions B.** v. 14, p. 191–205, 1983.

HESSEL, R. *et. al.* Determinação do módulo de Young em sólidos a partir da medida da velocidade do som pelo método do tempo de voo. **Revista Brasileira de Ensino de Física.** v. 38, n. 2 . 2016.

HOLMES, M.A.J. Bending and twisting friction models in soft-sphere discrete element simulations for static and dynamic problems. **Applied Mathematical Modelling.** v. 40, p. 3655 – 3670, 2016.

HUTCHINGS, I.; SHIPWAY, P. 3 – Friction. *In:* HUTCHINGS, I.; SHIPWAY, P. Tribology: Friction and Wear of Engineering Materials, 2 ed., Butterworth-Heinemann, 2017, p.37-77. Available in: < https://www.sciencedirect.com/science/article/pii/B9780081009109000039 >. Access: 01 May. 2022.

IDAGAWA, H. S. **Implementação de um simulador de partículas utilizando o Método dos Elementos Discretos (DEM) em cluster de GPUs.** 2017. Dissertation (Master's degree in Mechanical Engineering) - College of Mechanical Engineering, State University of Campinas, Campinas.

JASEVIČIUS, R. *et. al.* Numerical simulation of the sticking process of glass-microparticlesto a flat wall to represent pollutant-particles treatment in amulti-channel cyclone. **Particuology.** v. 32, p. 112–131, 2017.

JING, L.; STEPHANSSON, O. **Fundamentals of Discrete Element Methods for Rock Engineering:** Theory and Applications. Developments in Geotechnical Engineering, v. 85. Elsevier, Amsterdam, 562 p. 2007.

JUN, A. *et. al.* Assessment of rolling resistance models in discrete element simulations. **Powder Technology.** v. 206, p. 269 – 282, 2011.

KADKHODAIE, A.; KADKHODAIE, R. Acoustic, density, and seismic attribute analysis to aid gas detection and delineation of reservoir properties. **In: Sustainable Geoscience for Natural Gas Subsurface Systems: The Fundamentals and Sustainable Advances in Natural Gas Science and Eng**. Gulf Professional Publishing v.2, 2022, p. 51-92.

KATTERFELD, A. *et. al.* Calibration of DEM parameters for cohesionless bulk materials under rapid flow conditions and low consolidation. 2019.

KATTERFELD, A.; RÖSSLER, T. Standard procedure for the calibration of DEM parameters of cohesionless bulk materials. **Proceedings of the 8th international conference on discrete element methods (DEM8).** 2019.

KOMOSSA, H. *et. al.* Transversal bed motion in rotating drums using spherical particles: Comparison of experiments with DEM simulations. **Powder Technology**. v. 264, p. 96–104, 2014.

LI, Y. DEM simulations and experiments of pebble flow with monosized spheres. **Powder Technology.** v. 193, p. 312–318, 2009.

LU, R. *et. al.* Experiments and CFD-DEM simulations of cohesive particles sedimentation in stilled fluid. **Powder Technology.** v. 356, p. 222-230, 2019.

MA, Y. Z.; SOBERNHEIM, D; GARZON, J. R. Glossary for Unconventional Oil and Gas Resource Evaluation and Development. In: **Unconventional Oil and Gas Resources Handbook: Evaluation and Development.** Gulf Professional Publishing, 2016, p. 513-526.

MACHADO. S. S. **Tecnologia da Fabricação do Açúcar.** Inhumas: IFG; Santa Maria: Universidade Federal de Santa Maria, p. 56, 2012.

MARIGO, M; STITTI, E. H. Discrete Element Method (DEM) for Industrial Applications: Comments on Calibration and Validation for the Modelling of Cylindrical Pellets. **KONA Powder and Particle Journal.** n.32, p. 236–252, 2015.

MAXWELL, R. *et. al.* Computer simulations of particle–bubble interactions and particle sliding using Discrete Element Method. **Journal of Colloid and Interface Science.** v. 381, p. 1–10, 2012.

MCKENNA, H. A.; HEARLE, J.W.S.; O'HEAR, N. 4 - Properties of rope. *In:* MCKENNA, H. A.; HEARLE, J.W.S.; O'HEAR, N. Handbook of Fibre Rope Technology. In Woodhead Publishing Series in Textiles, 2004, p. 101-140. Available in: < https://www.sciencedirect.com/science/article/pii/B9781855736061500107 >. Access: 01 May. 2022.

MORENO-ATANASIO, R. Influence of the hydrophobic force model on the capture of particles by bubbles: A computational study using Discrete Element Method. **Advanced Powder Technology**. v. 24, p. 786–795, 2013.

NOROUZI, H. R. *et al.* **Coupled CFD-DEM Modeling:** Formulation, Implementation and Application to Multiphase Flows. 1st ed. Wiley-Blackwell, 2016.

O'SULLIVAN, C. Particle-Based Discrete Element Modeling: Geomechanics Perspective. **International Journal of Geomechanics**, p. 449-464, 2011.

PARAB, N. D. *et. al.* Fracture mechanisms of glass particles under dynamic compression. **International Journal of Impact Engineering.** v. 106, p. 146-154, 2017.

PARTELI, E. J. R. *et. al.* Attractive particle interaction forces and packing density of fine glass powders. **Scientific Reports.** v. 4, n. 6227, 2014.

PENG, B. **Discrete Element Method (DEM) Contact Models Applied to Pavement Simulation.** 2014. Dissertation (Master's degree in Civil Engineering)- Virginia Polytechnic Institute and State University, Virginia.

QI, F. *et. al.* Numerical study of particle mixing in a lab-scale screw mixer using the discrete element method. **Powder Technology.** v. 308, p. 334–345, 2017.

RAMÍREZ, A. *et. al.* Determination of the Mechanical Properties of Powdered Agricultural Products and Sugar. **Particle & particle systems characterization.** v. 26, p. 220 – 230, 2010.

RESNICK, R; HALLIDAY, D. Physics 1. 4th ed. v.1. Rio de Janeiro: LTC, 1983.

ROESSLER, T. *et. al.* Development of a standard calibration procedure for the DEM parameters of cohesionless bulk materials – part I: Solving the problem of ambiguous parameter combinations. **Powder Technology**. v. 343, p. 803-812, 2019.

SAKAI, M. *et. al.* Study on a large-scale discrete element model for fine particles in a fluidized bed. **Advanced Powder Technology.** v. 23, p. 673-681, 2012.

SAMPAIO, A.B. **O método dos elementos discretos com superelipsóides usando a parametrização das rotações de Rodrigues**. 2017. Dissertation (PhD in Structural Engineering) - University of São Paulo. Sao Paulo.

SAMUI, P.; SATYAM, N. Handbook of Research on Advanced Computational Techniques for Simulation - Based Engineering. In: SATYAM, N**. Liquefaction Modelling of Granular Soils using Discrete Element Method.** . 1ª. ed. Índia: IGI Global, 2016. cap. 15, p. 381-441.

SANTOS D. A. *et. al.* Transition Phenomenon Investigation Between Different Flow Regimes in a Rotary Drum. **Brazilian Journal of Chemical Engineering.** v. 33, n. 03, p. 491 – 501, 2016

SANTOS, L. *et. al.* Flow properties of coarse and fine sugar powders. **Wiley Periodicals: Journal Food Process Engineering**, 2017.

SATO, A. *et. al.* Experiment and simulation of the dry particle coating. **Chemical Engineering Science**, Elsevier, v. 86, p.164 - 172, 2011.

SINGH, D. et. al. Breakage functions of particles of four different materials subjected to uniaxial compression. Particulate Science and Technology. v. 34, n. 4, p. 494-501, 2016.

SONI, R. K. *et. al.* Numerical analysis of mixing of particles in drum mixers using DEM. **Advanced Powder Technology**. v. 27, p. 531–540, 2016.

SUHR, B; SIX, K. On the Effect of Stress Dependent Interparticle Frictionin Direct Shear Tests. **Powder Technology.** v. 294, p. 211–220, 2016

TAN, Z. et. al. Numerical analysis of electrostatic phenomena in gas-solid flow: A hybrid approach. **Powder Technology**. v. 354, p. 822-833, 2019.

TANG, T. *et. al.* Experimental Study and DEM Numerical Simulation of Dry/Wet Particle Flow Behaviors in a Spouted Bed. **Industrial & Engineering Chemistry Research.** 2019.

TIMOSHENKO, S.; GERE, J. **Mecânica dos Sólidos**. v.1, Rio de Janeiro: LTC, 1983.

TORBAHN, L. *et. al.* Mesostructural investigation of micron-sized glass particles during shear deformation – An experimental approach vs. DEM simulation. **Powders & Grains**. 2017.

ÚNICA. **Açúcar: importante fonte de energia**. Available in: < https://unica.com.br/setor-sucroenergetico/acucar/ >. Access: 01 Jun. 2022.

XU, Y. *et. al.* **2D DEM simulation of particle mixing in rotating drum: A parametric study. Particuology.** v. 8, p.141–149, 2010.

YARI, C. et al., Size segregation of bidisperse granular mixtures in rotating drum. **Powder Technology.** v. 374, p. 172-184, 2020.

YE, F. *et. al.* Calibration and verification of DEM parameters for dynamic particle flow conditions using a backpropagation neural network. **Advanced Powder Technology**. v.30. p. 292-301, 2019.

YEOM, S. B. et. al. Application of the Discrete Element Method for Manufacturing Process Simulation in the Pharmaceutical Industry. **Pharmaceutics.** v.11, n. 8, 2019.

ZHOU, L. *et. al.* DEM Parameter Calibration of Maize Seeds and the Effect of Rolling Friction. **Processes**. 2021.

ZHOU, Y. C. *et al.* An experimental and numerical study of the angle of repose of coarse spheres. **Powder Technology.** v. 125, p. 45–54, 2002.

ZHOU, Y. C.; XU, B.H.; YU, A. B. Numerical investigation of the angle of repose of monosized spheres. **Physical Review E.** v.64, p. 021301-1 - 021301-8, 2001.

ZHU, H. P. *et al.* Discrete particle simulation of particulate systems: Theoretical developments. **Chemical Engineering Science**. v. 62, p. 3378–3396, 2007.

APPENDIX 1 - CASE STUDY SCRIPT

```
atom_style    granular
atom_modify   map array
boundary      f f f
newton        off

communicate   single vel yes

units         si

region        domain block -0.2 0.2 -0.2 0.2 -0.2 0.2 units box
create_box    2 domain

neighbor      0.002 bin
neigh_modify  delay 0
hard_particles yes

fix  m1 all property/global youngsModulus peratomtype 5.5e10 5.5e10
fix  m2 all property/global poissonsRatio peratomtype 0.25 0.25


fix  m3 all property/global coefficientRestitution peratomtypepair 2 0.67 0.67 0.67 0.67
fix  m4 all property/global coefficientFriction peratomtypepair 2 0.57 0.57 0.57 0.57
fix  m5 all property/global coefficientRollingFriction peratomtypepair 2 0.05 0.05 0.05 0.05

pair_style  gran model hertz tangential history #Hertzian without cohesion
pair_coeff  * *

timestep    0.000001

fix  gravi all gravity 9.81 vector 0.0 0.0 -1.0

fix  cad all mesh/surface/stress file meshes/cilindro.stl type 1 scale 1
fix  cad2 all mesh/surface/stress file meshes/plano.stl type 1 move 0 0 0 scale 1 rotate axis 0. 0. 1 angle
90.
fix  inface all mesh/surface file meshes/insertion_face.stl type 1 scale 0.8 move 0.015 0.05 0
fix  granwalls all wall/gran model hertz tangential history mesh n_meshes 2 meshes cad cad2

fix   pts1 all particletemplate/sphere 15485863 atom_type 1 density constant 2456 radius constant
0.00507
fix   pts2 all particletemplate/sphere 15485867 atom_type 2 density constant 2456 radius constant
0.00507

fix  pdd1 all particledistribution/discrete 32452843  1 pts1 1.0
fix  pdd2 all particledistribution/discrete 32452843  1 pts2 1.0

compute       1 all erotate/sphere
thermo_style  custom step atoms ke c_1 vol
thermo        1000
thermo_modify lost ignore norm no
dump   dmp all custom/vtk 25000 post/particulas_*.vtk id type type x y z ix iy iz vx vy vz fx fy fz omegax
omegay omegaz radius
dump   dumpstress all mesh/gran/VTK 25000 post/mesh_*.vtk stress wear cad cad2 inface

group  nve_group region domain

fix    integr nve_group nve/sphere
```

```
fix     ins nve_group insert/stream seed 32452867 distributiontemplate pdd1 &          nparticles 600 massrate 1 insert_every 100000 overlapcheck yes all_in no vel constant 0.0 0.0 -1.0 & insertion_face inface
run    1000000
unfix  ins

run 10000

fix                     movecad2 all move/mesh mesh inface  linear  0 -1 0
run 100000
unfix movecad2

fix     ins2 nve_group insert/stream seed 32452867 distributiontemplate pdd2 &          nparticles 600 massrate 1 insert_every 100000 overlapcheck yes all_in no vel constant 0.0 0.0 -1.0 & insertion_face inface

run    1000000
unfix  ins2
run 10000

fix                     movecad3 all move/mesh mesh cad2  linear  -1 0 0
run 105000
unfix movecad3

run 10000
fix                     movecad all move/mesh mesh cad rotate origin 0. 0. 0. axis 1. 0. 0. period 0.75.
run 10000000
```

APPENDIX 2 – SCRIPT FOR GRANULATED SUGAR

```
atom_style    granular
atom_modify   map array
boundary      f f f
newton        off

communicate   single vel yes

units         si

region        domain block -0.05 0.05 -0.05 0.05 -0.05 0.05 units box
create_box    1 domain

neighbor      0.002 bin
neigh_modify  delay 0

fix  m1 all property/global youngsModulus peratomtype 4.5e8

fix  m2 all property/global poissonsRatio peratomtype 0.252

fix  m3 all property/global coefficientRestitution peratomtypepair 1 0.16

fix  m4 all property/global coefficientFriction peratomtypepair 1 0.25

fix  m5 all property/global coefficientRollingFriction peratomtypepair 1 0.0

pair_style  gran model hertz tangential history rolling_friction epsd2
pair_coeff  * *

 timestep    0.000001

fix  gravi all gravity 9.81 vector 0.0 0.0 -1.0

fix  cad all mesh/surface/stress file meshes/Drum.stl type 1 scale 1 rotate axis 1. 0. 0 angle 90.
fix  cad2 all mesh/surface/stress file meshes/Glass.stl type 1 scale 1 rotate axis 1. 0. 0 angle 90.
fix  inface all mesh/surface file meshes/insertion_face.stl type 1 scale 0.8 rotate axis 1. 0. 0 angle 90.
fix  granwalls all wall/gran model hertz tangential history mesh n_meshes 2 meshes cad cad2

compute       1 all erotate/sphere
thermo_style  custom step atoms ke c_1 vol
thermo        1000
thermo_modify lost ignore norm no
dump   dmp all custom/vtk 25000 post/particulas_*.vtk id type type x y z ix iy iz vx vy vz fx fy fz
omegax omegay omegaz radius
dump   dumpstress all mesh/gran/VTK 25000 post/mesh_*.vtk stress wear cad cad2 inface

group  nve_group region domain

fix    integr nve_group nve/sphere

fix  pts1 all particletemplate/sphere 15485863 atom_type 1 density constant 1570 radius constant
0.00053

fix  pdd1 all particledistribution/discrete 32452843  1 pts1 1.0

fix    ins nve_group insert/stream seed 32452867 distributiontemplate pdd1 &
       nparticles 20355 massrate 0.01 insert_every 100000 overlapcheck yes all_in no vel constant 0.0
0.0 -0.1 &
```

```
      insertion_face inface
run    1000000
unfix  ins

fix movecad2 all move/mesh mesh inface  linear  -6 0 0
run 100000
unfix movecad2

run 10000
fix movecad all move/mesh mesh cad rotate origin 0. 0. 0. axis 0. 1. 0. period 2.
run 2000000
```